PREPARATION AND CHARACTERIZATION OF ALUMINUM COMPOSITE CLOSED-CELL FOAMS

by
Semih Elbir

A Dissertation Submitted to the
Graduate School in Partial Fulfillment of the
Requirements for the Degree of

MASTER OF SCIENCE

Department: Materials Science and Engineering
Major: Materials Science and Engineering

İzmir Institute of Technology
İzmir, Turkey

September, 2001

We approve the thesis of **Semih ELBİR**

Date of Signature

..... **26.09.2001**

Asst. Prof. Mustafa GÜDEN

Supervisor

Department of Mechanical Engineering,

..... **26.09.2001**

Asst. Prof. Selahattin YILMAZ

Co-Supervisor

Department of Chemical Engineering,

..... **26.09.2001**

Prof. Dr. Devrim BALKÖSE

Department of Chemical Engineering,

..... **26.09.2001**

Asst. Prof. Metin TANOĞLU

Department of Mechanical Engineering,

..... **26.09.2001**

Asst. Prof. Hacer AYGÜN

Department of Mechanical Engineering,

..... **26.09.2001**

Prof. Dr. Muhsin ÇİFTÇİOĞLU

Head of Interdisciplinary

Materials Science and Engineering Program

ACKNOWLEDGEMENT

I wish to express my sincere gratitude to my advisors Asst. Prof. Mustafa Güden and Asst. Prof. Selahattin Yılmaz for their supervisions, guidance, encouragement and supports in the experimental study and during the course of this study. Without their help and friendship, this thesis could have never been finished.

I would like to thank Prof. Dr. Muhsin Çiftçioğlu for his comments and suggestions during my assistantship and thesis. I would like to add my special gratitude to my roommates, my assistant friends and laboratory technicians. I am also grateful to the support provided by TÜBİTAK (Project no:MİSAG-135).

Finally, I would like to thank my family for their understanding, encouragement and support.

ABSTRACT

An experimental study has been conducted to investigate the feasibility of the production of SiC-particulate (SiC_p) reinforced Al (Aluminum) closed-cell foams using the foaming from powder compacts process and to determine the effect of SiC_p addition on the foaming behavior of Al compacts and the mechanical properties of Al foams. The foaming behavior of SiC_p/Al composite powder compacts and the compression mechanical behavior of SiC_p/Al composite foams were determined and compared with those of pure Al compacts and Al foams prepared by the same processing parameters.

Composite and Al powder compacts were prepared by hot uniaxial compaction inside a steel die at 425 ^oC for 1/2 hour under a constant die pressure of 220 MPa. Compacts of 99 % dense with a small amount of blowing agent of TiH_2 (0.5 wt%) were heated above the melting temperature of Al inside a pre-heated furnace. During heating, as the TiH_2 decomposed and released hydrogen, the compact expanded uniaxially. Foamed/partially foamed samples were taken from the furnace at the specified furnace holding times and their heights were measured in order to calculate linear expansion.

Initial foaming experiments with Al compacts at 750 and 850 ^oC have shown that foaming at the former temperature was slower and more controllable, although linear expansion was similar at both temperatures. From these experiments, it was also found that rapid cooling of the liquid metal was necessary in order to maintain the liquid foam structure in the solid state.

Foaming experiments of SiC_p/Al and Al compacts at 750 ^oC have shown that SiC_p addition a) increased linear expansion of the powder compacts and b) reduced the extent of liquid metal drainage. SiC_p addition also increased the plateau stress and energy absorption capability of the Al foams. These results have shown the potential of composite foams for tailoring energy absorption of Al foams for varying levels of impact stresses.

Foaming experiments have also been conducted on aluminum oxide-particulate/Al and SiC-whisker/Al composites compacts prepared using the same compaction parameters and foamed at the same temperature, 750 ^oC.

ÖZ

Toz tabletlerden köpükleştirme yöntemi ile SiC-parçacık (SiC_p) takviyeli kapalı hücreli alüminyum (Al) köpüklerin üretim fizibilitesini incelemek ve SiC_p katkısının Al tabletlerinin köpükleşmesine ve üretilen köpüklerin mekanik özelliklerine etkilerini belirlemek için deneysel bir çalışma yapılmıştır. SiC_p/Al kompozit toz tabletlerin köpükleşme ve üretilen kompozit köpüklerin ise basma altında mekanik davranışları belirlenmiş ve bunlar saf Al tabletlerin köpükleşme ve Al köpüklerin mekanik davranışları ile karşılaştırılmıştır.

Kompozit ve Al toz tabletler 425 ^oC'de çelik bir kalıp içerisinde ve sabit bir basınç altında (220 MPa) sıcak presleme metoduyla hazırlanmıştır. Nispi yoğunluğu %99'a ulaşan ve içerisinde % 0.5 (ağırlık yüzdesi) TiH_2 (titanyum hidrür) bulunan tabletler Al metalinin erime sıcaklığının üstüne ısıtılmış bir fırında köpükleştirilmiştir. Isıtılma esnasında, TiH_2 bozunarak hidrojen gazı çıkartırken, tablet tek yönde genleşmektedir. Belirli fırında kalma sürelerinde köpükleşmiş veya kısmi köpükleşmiş numuneler fırından alınarak soğutulmuş ve boyutları ölçülerek doğrusal uzama hesaplanmıştır.

Al tabletlerle 750 ve 850 ^oC'de yapılan ön köpükleşme deneyleri, her iki sıcaklıkta da doğrusal uzamanın benzer olduğunu göstermesine karşın, 750 ^oC'de köpükleşmenin daha yavaş ve kontrollü olduğunu göstermiştir. Yine bu deneyler sonucunda, sıvı metal köpük yapısının katı halde de korunması için sıvı metalin hızlı soğutulması gerektiği bulunmuştur.

SiC_p/Al ve Al tabletlerle 750 ^oC'de yapılan köpükleştirme deneyleri, SiC_p takviyesinin; a) toz tabletlerde doğrusal uzamayı arttırdığını ve b) köpükleşme esnasında sıvı metalin aşağı doğru akmasını azalttığını göstermiştir. SiC_p takviyesi ile Al köpüklerin plato gerilmeleri ve enerji emme kapasiteleri de artmıştır. Bu sonuçlar, değişen darbe gerilmelerinde, kompozit yapıların uygun köpük malzemesinin seçilmesinde kullanılabileceğini göstermektedir.

Benzer paketleme parametreleri ile hazırlanan alüminyum oksit parçacık/Al ve SiC-viskır/Al kompozit tabletler de 750 ^oC'de köpükleştirilmeye çalışılmıştır.

TABLE OF CONTENTS

LIST OF FIGURES

LIST OF TABLES

Chapter I

INTRODUCTION

Aluminum (Al) closed-cell foams are materials of increasing importance because they have good energy absorption capabilities, as well as other properties such as damping, insulation, specific stiffness and fire retardant properties [1]. They can convert much of impact energy into plastic energy and absorb more energy than bulk metals. When used as filling materials in tubes, they increase total energy absorption over the sum of the energy absorbed by foam alone plus tube alone [2, 3, 4]. Plastic deformation or yielding starts at a stress called plateau stress. Plateau stress, more or less, determines the maximum load that should be exerted on a protected structure or device and the associated amount of energy that should be absorbed [5]. Therefore, foams with higher plateau stresses may be preferred for the applications of increasing impact stresses in order to increase protection level.

It has been found that morphologic imperfections such as cell wall wiggles and curves, cell elipticity and inhomogeneous cell thickness and cell size distribution tend to decrease the plateau stress; hence the energy absorption capability [6, 7]. Improving foam structure, for example increasing the aspect ratio of cell wall thickness against cell edge thickness, has been found to elevate plateau stress and also is expected to result in a more uniform plateau stress [5, 8]. Besides cell morphology, foam density and foaming alloy yield stress are the two other parameters that will affect plateau stress. Utilization of higher yield strength Al alloy may be more appropriate than increasing foam density for higher plateau stresses, because in the former density; hence weight remain constant as strength increases. An alternative way of increasing foaming alloy strength might be including small ceramic reinforcing phase such as SiC-particulates (SiC_p), Al_2O_3-particulates (Al_2O_{3p}) and SiC-whiskers (SiC_w) to the Al alloy in order to form Metal Matrix Composite (MMC) foam structure. This study is ,therefore, conducted in order to investigate the foaming and the mechanical properties of SiC_p MMC Al foams and to compare them with those of pure Al foams prepared with the same processing parameters in order to determine the effect of SiC_p on foaming and mechanical properties of Al foams. Composite and pure Al foams were prepared using a powder metallurgical process known as *foaming from powder compacts* developed by

Fraunhofer Resource Center [9]. According to our knowledge, composite structures have not been investigated with this method yet, although in a foam production process by Cymat, SiC_p are added to the liquid Al metal prior to foaming in order to enhance viscosity of the melt [10] and therefore foams produced by this process have MMC structure. However, the effect SiC_p on the mechanical behavior of Al foams produced by this process have not been extensively investigated yet. This study also serves for the purpose of investigating the feasibility of manufacturing of composite foams using the *foaming from powder compacts* process.

Chapter II

PRODUCTION PROCESSES OF ALUMINUM CLOSED-CELL FOAMS

Currently there are three commercial Al closed-cell foam production processes: 1) foaming of melts by gas injection 2) foaming of melts with blowing agents and 3) foaming from powder compacts.

2.1 Foaming of Melts by Gas Injection

This process is currently applied by Alcan N. Hydro (Norway) and Cymat Aluminum Corporation (Canada) [10, 11]. In this process, ceramic particles e.g. SiC, Al_2O_3, or magnesium oxide, are added in order to enhance the viscosity of the liquid metal to be foamed. In the second step, the melt is foamed by injecting gas (air or nitrogen) using rotating air injection shaft which generates fine gas bubbles and distributes them homogeneously in the melt (Figure 2.1) [12]. Since the bubbles are stabilized by ceramic particles, they can be pulled off melt surface using a conveyor belt. Finally, the foam is cooled down below the melting point of the metal matrix.

Typical volume fraction range of the ceramic particles used in the process is between 10 and 20% with a mean particle size between 5μm and 20 μm as depicted in Figure 2.2 [11, 13]. Typical density, average cell size and cell wall thickness are 0.069-0.54g/cm^3, 3-25 mm, and 50-85 μm, respectively [12]. Average cell size, average cell wall thickness and density can be adjusted by varying processing parameters including gas injection rate and rotating shaft speed.

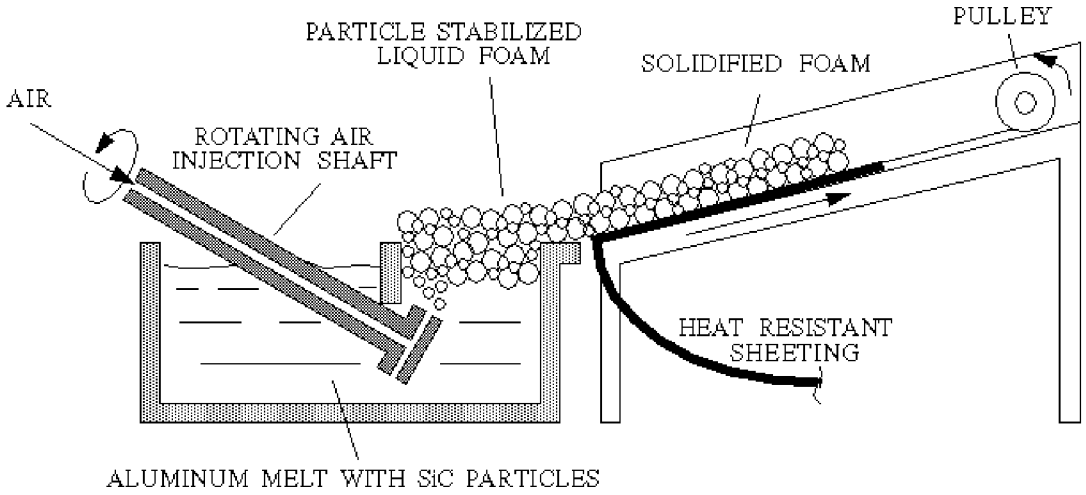

Figure 2.1 Foaming of melt by gas injection.

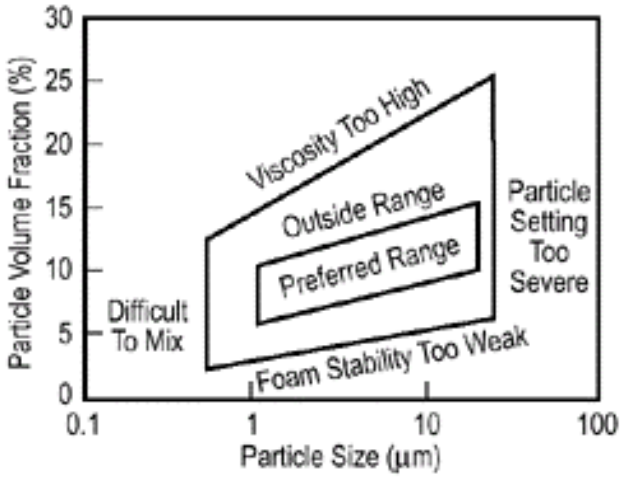

Figure 2.2 Preferable particle volume fraction and particle size range of stabilizing powders.

Drainage is observed in the foamed slabs, which causes gradient in density, and pore size. The conveyor belt also induces shearing forces, leading to the formation of elongated cells [10]. Solidified foams contained a dense outer surface layer can be used directly or machined into any desired shape. However, machining of these foams may be difficult due to the presence of hard ceramic particles, in the metal matrix.

The process has the capability for continuous production of large volumes of low density and MMC foams at a relatively lower cost. The disadvantage of direct foaming is the necessity for the secondary processes such as cutting and machining.

2.2 Foaming of Melts with Blowing Agents

The second process of Al closed-cell foam production is to add a foaming agent or blowing agent (TiH_2) into liquid metal. As the foaming agent decomposes, the released hydrogen (H_2) gas drives the foaming process (Figure 2.3) [14, 15]. Before foaming, 1.5 wt.% calcium metal is added into the liquid Al at 680 ^oC and then the melt is stirred quickly (Figure 2.3) [14]. The viscosity of the melt increases with increasing stirring time because of the formation of oxide and/or metallic compounds (calcium oxide, calcium-aluminum oxide, or Al_4Ca intermetallic) which thicken the metallic melt [16]. The effects of calcium volume fraction and stirring time on the viscosity of an Al melt are shown in Figure 2.4 [15]. In a later stage of the process, after adjusting the viscosity of the liquid metal, TiH_2 with an amount of 1.6 wt.% is added into the melt, which releases hydrogen gas in the hot viscous liquid according to the following reaction:

$$TiH_2\ (s) \rightarrow Ti\ (s) + H_2\ (g)$$

This results in the expansion of the liquid metal and filling of the foaming vessel with liquid foam at a constant pressure. Finally, the liquid foam is cooled down below the melting point of the foamed alloy quickly and the solidified Al foam is further processed for specific applications.

The Al foams produced by the process, *Alporas*^{TM}, is the most homogeneous foams produced currently [15]. Typical densities of the cast foams are between 0.18 g/cm^3 and 0.24 g/cm,^{3} with an average pore size ranging from 2 mm to 10 mm [14, 15]. The viscosity of the molten Al can also be adjusted by injecting oxygen, air and other gas mixtures through the melt which cause formation of Al_2O_3 particles and by adding viscosity enhancing additives directly such as aluminum oxide and SiC. Complicated temperature cycles, difficulty in adjustment of the variables and the need for secondary processing (machining) are the disadvantages of the process.

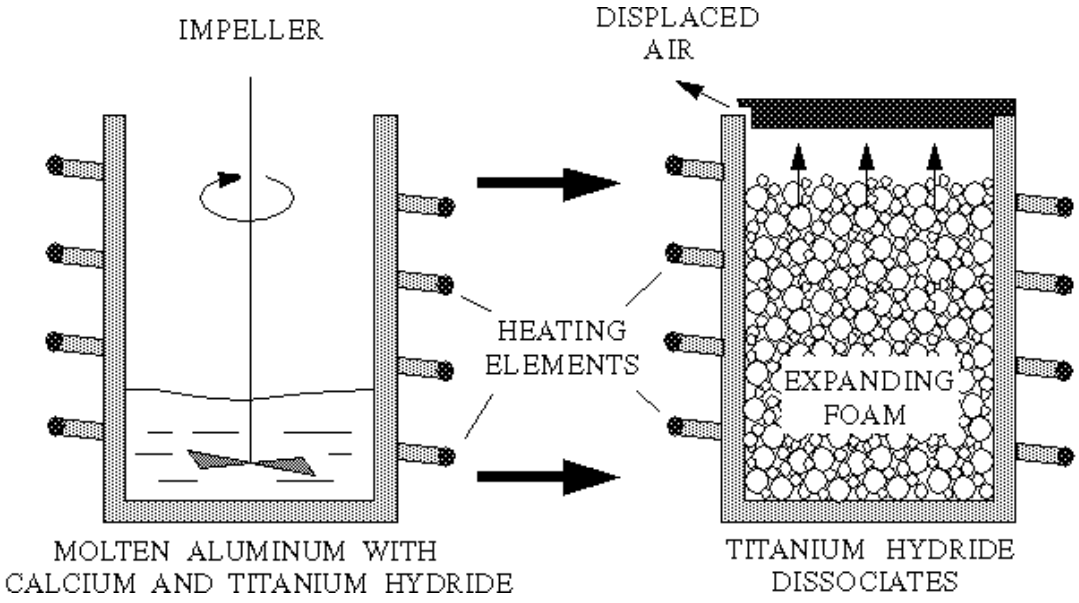

Figure 2.3 Direct foaming of melts by adding gas-releasing agent.

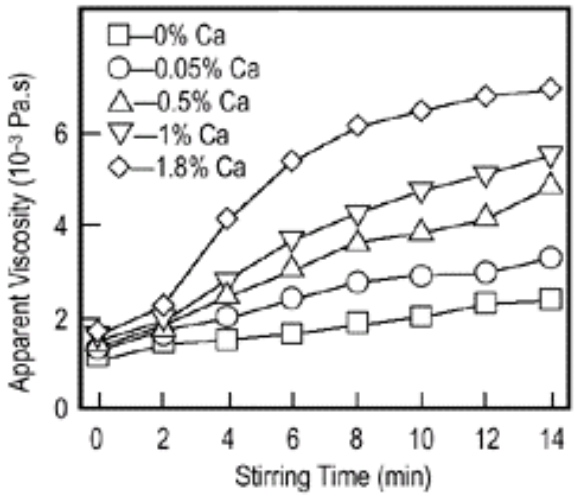

Figure 2.4 Effect of calcium (Ca) fraction and stirring time on the viscosity of liquid Al metal.

2.3 Foaming from Powder Compacts

The process starts with mixing metal powders with a blowing agent which upon heating releases a foaming gas (Figure 2.5) [17]. Metal powder-blowing agent mixture is then compressed to a dense, semi-finished foamable product via metal forming processes such as hot compaction, extrusion and rolling (Figure 2.5). In a final step, the semi-finished product is heated to a temperature near to the melting point of the metal. During heating, the blowing agent decomposes and subsequently releases gas, leading to the expansion of the molten or mushy metal and the formation of a highly porous structure.

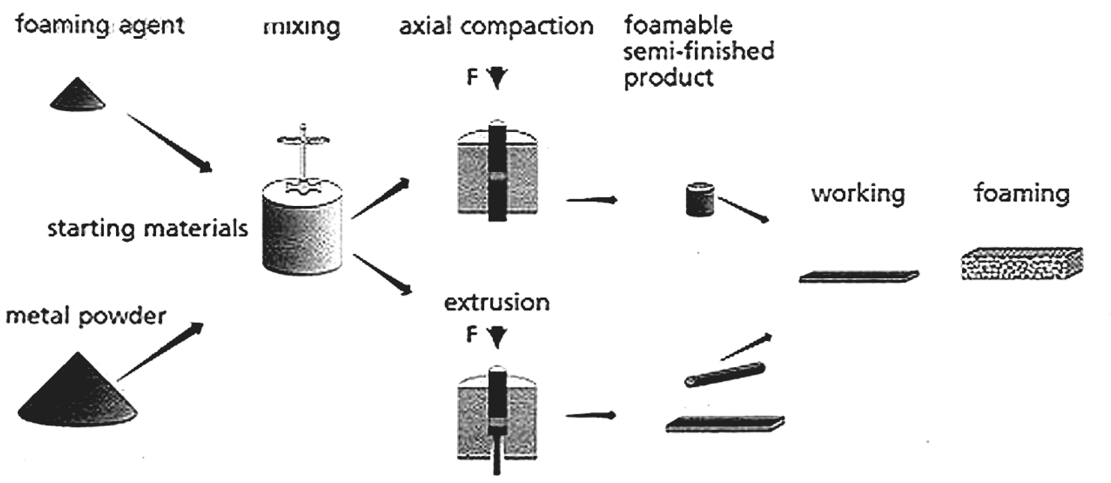

Figure 2.5 Foaming from powder compacts process.

Besides metal hydrides (e.g., TiH_2), carbonates (e.g., calcium carbonate, potassium carbonate, sodium carbonate and sodium bicarbonate), hydrates (e.g., aluminum sulphate hydrate and aluminum hydroxide) or substances that evaporate quickly (e.g., mercury compounds or pulverized organic substances) can also be used as blowing agent.

For an efficient foaming, it is very critical to form a gas-tight semi finished product in which the blowing agent is entrapped fully in the metallic matrix. Therefore the temperature and the pressure of hot compaction must be high enough to bond the individual metal powder particles and form a gas-tight seal around the blowing agent particles so that early decomposition of the blowing agent and the escape of H_2 gas before the melting of semi-finished product are avoided. In compaction by rolling, a

temperature range between 350 ^{o}C and 400 ^{o}C is sufficient for the diffusion between the particles especially in the surface layers [17].

The amount of blowing agent for foaming of Al and its alloys have been found to be small. Calculations have shown that 0.6 wt.% TiH_2 in a foamable Al compact would give an expansion factor of 17, a value almost 4 times higher than the expansion factor (4-5) experimentally found [9]. This indicates that, only 25% of the released hydrogen is effective in forming pores, and the rest is lost during foaming.

The time needed for full expansion of the semi-finished product depends on the temperature and size of the precursor and ranges from a few seconds to several minutes. The process is not only restricted to Al and its alloys, but also tin, zinc, brass, lead, gold, and some other metals and alloys can also be foamed using appropriate blowing agents and process parameters [18].

If a piece of foamable product is foamed in a furnace, the result will be a lump of metal foam with an undefined shape unless the expansion is limited. This is done by inserting the semi-finished foamable material into a hollow mold and expanding it by heating (Figure 2.6). This process results in near-net shaped parts with a closed and dense outer skin and a highly porous cellular core. Complicated parts can be manufactured by pouring the expanding liquid foam into a mold (Figure 2.7 (a)). Sandwich panels consisting of a foamed metal core and two metal face sheets can be manufactured by bonding the face sheets to a piece of foam with adhesives. Another way is to roll clad Al or steel sheets into a sheet of foamable material and allow the foamable core to expand while the face sheets remain dense (Figure 2.7 (b)) [19]. By this method, Al foam structures can be combined with steel or titanium face sheets as well as with Al face sheets. In the latter case, Al sheets with melting points that are higher than the core material must be used to avoid melting of the face sheets during foaming.

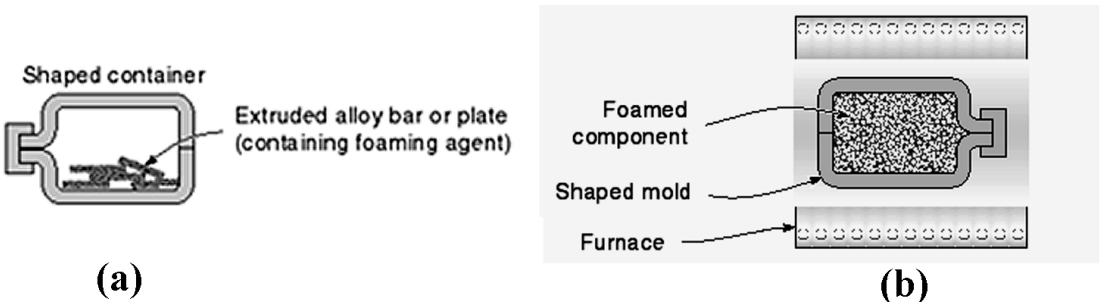

Figure 2.6 Foaming inside a mold a) inserting precursor material and b) foaming in the mold.

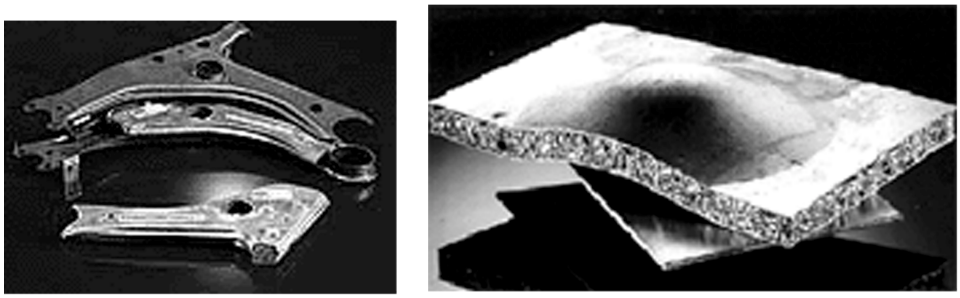

Figure 2.7 a) a complicated foam part and b) sandwich foam structure.

It is possible, with this process by applying suitable heating, to produce bodies that have continuously or discontinuously changing densities over the cross section. If the foaming process is interrupted after a certain time at a constant temperature, a certain density will be obtained and if the foaming process is continued further, a higher density value will result. For example, structures having higher foam densities on the locations exposed to higher external loads could be manufactured by this method. If the hot compaction process is performed inside a mold, the powder mixture will be surrounded completely or partially by a blowing agent free metal powder. Upon foaming, this forms a dense or less porous cover layer and a highly porous foam core. This offers advantages for the joining similar or different structures and for the production of foam core structures that require a dense cover such as car doors and frames.

Foaming from powder compacts process has been recently modified by incorporating TiH_2 particles directly into an Al melt instead of using powders to prepare a foamable precursor material. To avoid premature H_2 evolution, the melt should be quickly cooled down below its melting point after mixing or the blowing agent has to be passivated to prevent it from releasing gas before solidification. The former technique, called *Foamcast* is carried out in a die-casting machine and the powdered hydride is injected into the die simultaneously with the melt [20]. The resulting cast part is virtually dense and could be foamed by remelting in analogy to foaming from powder compacts; however, achieving a homogeneous distribution of TiH_2 powders in the die is difficult. The latter route requires that TiH_2 powders be subjected to a heat treatment cycle that forms an oxide layer on each particle, which delays the decomposition of TiH_2. TiH_2 is then added to the melt and the melt can be cooled at comparatively slow rates after stirring. Melts containing SiC_p are used to obtain stable foams. The name

Formgrip has been given to this process which is an acronym of foaming of reinforced metals by gas release in precursors. [22]

Chapter III

MECHANICAL PROPERTIES OF CLOSED-CELL ALUMINUM FOAMS

Closed-cell Al foams have unique mechanical properties such as high weight to strength ratios, good energy absorption capabilities and zero Poisson's ratios, which make them materials to be used potentially in various kinds of engineering applications [22, 23, 24, 25]. Among many other properties, deformation under compressive loads, elastic deformation, collapse or plateau stress, indentation and energy absorption properties are the most important and widely studied. These are briefly reviewed in this chapter and Al foams are particularly emphasized, but most of the properties considered could also be applied to the foams of other metals.

3.1 Deformation under compressive loads

Closed-cell foam structured Al metals show a characteristic compressive stress-strain curve. As depicted in Figure 3.1 for a 6061 Al foam, it consists of three distinct regions: linear elastic, collapse and densification [26]. In linear elastic region deformation is controlled by cell wall bending and/or stretching. This region is followed by a collapse region occurring by several different mechanisms, i.e. elastic buckling and brittle crushing of cell walls and formation of plastic hinges. Deformation in this region is highly localized and proceeds by the spreading of deformation from localized to undeformed regions of the sample. Since the deformation is localized, large oscillations in stress occur due to the repetitive nature of the process of cell collapse and densification (Figure 3.1). Collapse region is characterized by a stress plateau either with a constant value or increasing slightly with strain, for example see Figure 3.1. At a critical strain, ε_d, cell walls start to touch each other and, as a result of this, the material densifies (densification region). The stress in this region increases sharply and approaches to the strength of the bulk Al metal.

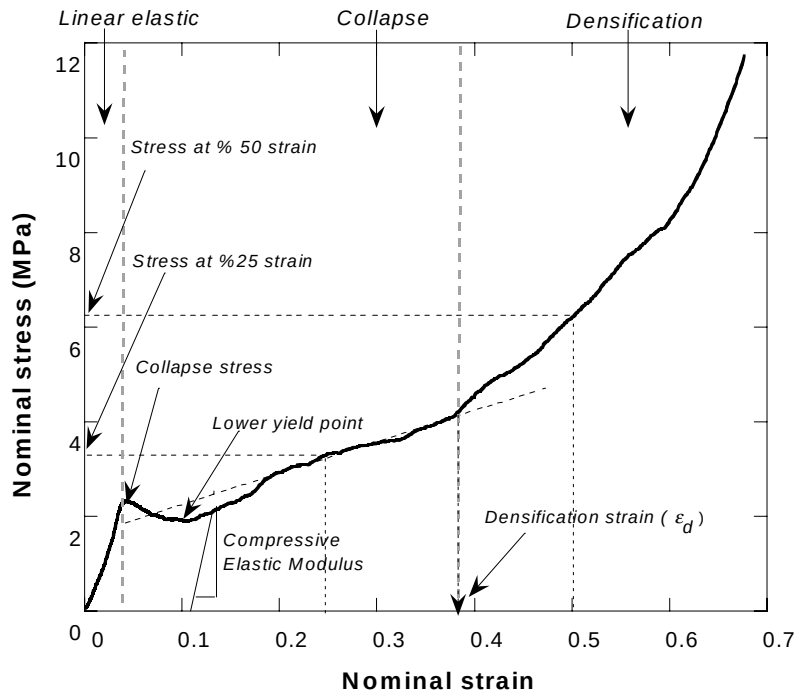

Figure 3.1 Compressive stress-strain curve of a 6061 Al foam.

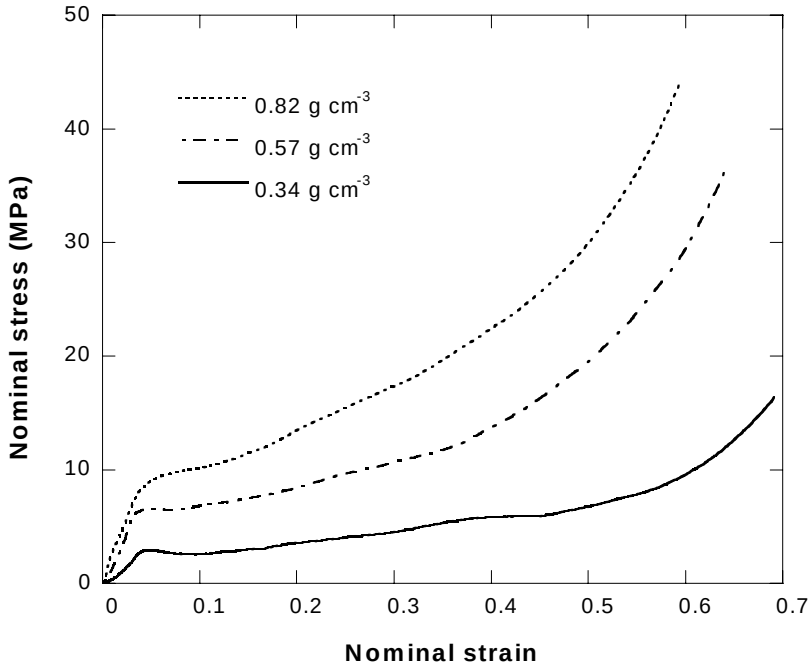

Figure 3.2 Compressive stress-strain curve of 6061 Al foam at various densities.

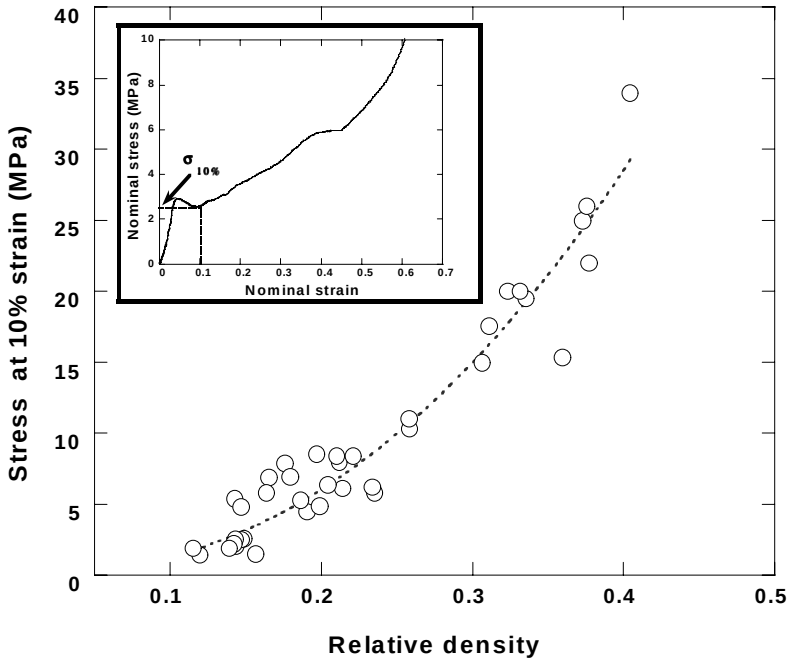

Figure 3.3 Variation of compressive stress at 10% strain of a 6061 Al foam with relative density.

Compressive mechanical properties of Al foams depend on their density and yield strength of the alloy which they are made of. Compressive stress or plateau stress generally increases with increasing density (Figure 3.2 and 3.3) [27, 28] and increasing with yield strength of the foam material.

3.2 Elastic Properties

Gibson and Ashby, using simple cubic models of beams (Appendix A), derived [1]

$$\frac{E^*}{E_s} = \alpha_1 \rho \tag{3.1}$$

and

$$\frac{E^*}{E_s} = \alpha_2 \rho^2 \tag{3.2}$$

for ideal closed-cell and open cell foams respectively. In these equations, E* and E_s are the Elastic Modulus of the foam and cell wall material, respectively. The relative density, ρ, is defined as

$$\rho = \frac{\rho^*}{\rho_s} \tag{3.3}$$

where ρ* and ρ_s are the densities of foam and cell wall material, respectively. The values of coefficients $\propto_1$ and $\propto_2$ depend on the geometric arrangement of cells. The value of $\propto_1$ is calculated to be 1/3 for isotropic closed-cell foams [5], 0.35 for tetrakaidecahedron cells and face centered cubic packed hollow spheres and unity for honeycombs [29]. The value of $\propto_2$ nearly equals to unity [30].

Experimentally measured moduli values of commercial Al closed-cell foams are much lower than those predicted by Equation 3.1 especially at relatively low foam densities [31]. The moduli degradation is partly due to the thicker regions of the material on cell edges as compared to cell walls because surface tension tends to draw liquid metal to the intersections during foaming process. Including cell material distribution between cell walls and edges, Gibson and Ashby proposed the following equation for the modulus of imperfect closed-cell foams [1]

$$\frac{E^*}{E_s} = C_1 \varphi^2 \rho^2 + C_2 (1 - \varphi) \rho \tag{3.4}$$

Here, φ is the fraction of the material contained on cell edges and C_1 and C_2 are geometrical coefficients similar to α_1 and α_2. The first and the second terms of the Equation 3.4 are due to cell edge bending and cell wall stretching, respectively. A high value of φ, generally found in commercial Al closed-cell foams (0.92-0.94 for Alulight)

[32], implies that modulus is dominantly determined by the cell edge bending; therefore, closed-cell foams behave as if their cells were open. Experimentally measured moduli data of closed-cell foams are usually fitted to the following general equation,

$$\frac{E^*}{E_s} = \alpha \rho^n \tag{3.5}$$

Typical value of n is 1.5-2 for Alulight foams [33] and the value of α is 3 for the higher quality foams and 1/2 for inferior foams [5].

Curved, wrinkled and missing cell walls, voids on the cell edges and cell walls and non-uniform density are the further imperfections degrading mechanical properties of closed-cell Al foams [6, 34, 35]. Foams may also show anisotropy in mechanical properties resulting from ellipsoidal cell shape. The shear stress between conveyer belt and liquid foam induces an ellipsoidal cell shape in Cymat foams [36] and Fraunhofer foam cells are claimed to be elongated in the plane perpendicular to compaction direction [37].

The effect of enclosed gas pressure on mechanical properties is usually ignored for Al closed-cell foams because cell walls crush during compression. Therefore, the enclosed gas escapes through the cell walls.

3.3 Plastic Collapse and Densification

The collapse stress or plateau stress (average stress in collapse region of Figure 3.1) is an indication for the progression of the inelastic and inhomogeneous deformation. As explained later in this chapter, it determines the amount and the efficiency of plastic energy absorption. For an ideal closed cell structure, plastic collapse is expected to occur by the cell wall stretching in a direction perpendicular to compression axis and the plateau stress is given as [1] (Appendix A)

$$\frac{\sigma_{pl}^*}{\sigma_{ys}} = C\rho \tag{3.6}$$

where, C is a geometrical constant. In the case of cell buckling and membrane stretching occurring simultaneously, the plateau stress is given as [1]

$$\frac{\sigma_{pl}^{*}}{\sigma_{ys}} = C_5 \quad \varphi \frac{\rho^{*}}{\rho_s} \qquad ^{3/2} + C_6''(1 \quad \varphi) \ \frac{\rho^{*}}{\rho_s} \tag{3.7}$$

Here, again C_5 and C_6 are geometrical coefficients. If the cell walls are thin enough to crumple in the compression direction with a very small force, strength will be dominated by the cell edge bending and approach to the strength of open cell foams. If not, they will stretch at right angle to loading direction and may significantly contribute to yield strength of the foam. A high value of φ together with imperfections degrades the plateau stresses of commercial Al closed-cell foams.

3.4 Indentation

Similar to bulk metals, metal foams show a higher strength in indentation than in uniaxial compression, (Figure 3.4) [38]. During indentation, an additional energy consumed as the indenter tears the foam around the perimeter. The region under the indenter collapses at a stress of compression plateau stress (Figure 3.5) [38]. The tear energy added to the plateau stress determines the indentation pressure [39]

$$\frac{F}{\pi a^2} = \bar{P} = \sigma_{pl}^{*} + \frac{2\gamma}{a} \tag{3.8}$$

where, F, P, γ and a are the total force applied, indentation pressure, tear energy and indenter radius, respectively. The indentation pressure is the function of indenter size and foam density. As the indenter size increases, the indentation pressure decreases until indentation pressure reaches to the plateau stress [39].

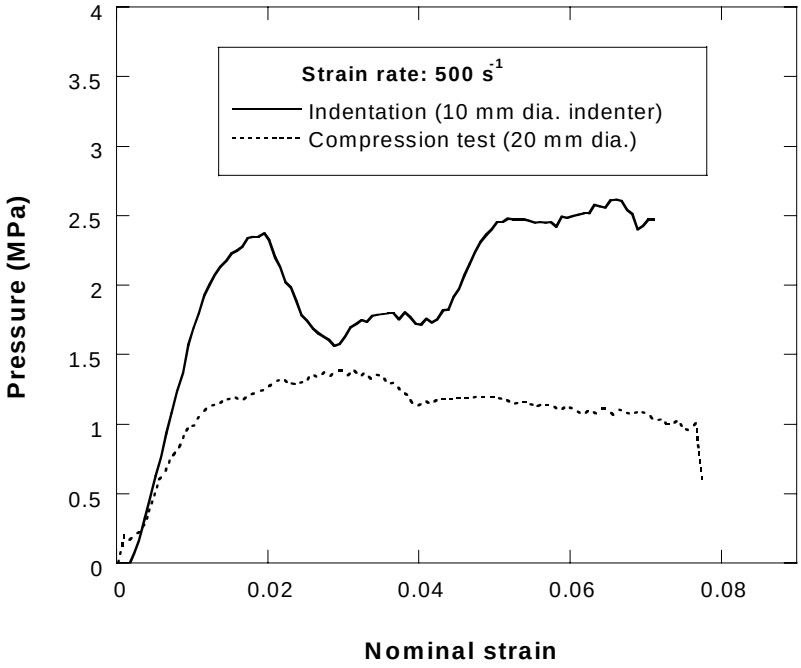

Figure 3.4 High strain rate stress-strain curves showing the difference between compression and indentation .

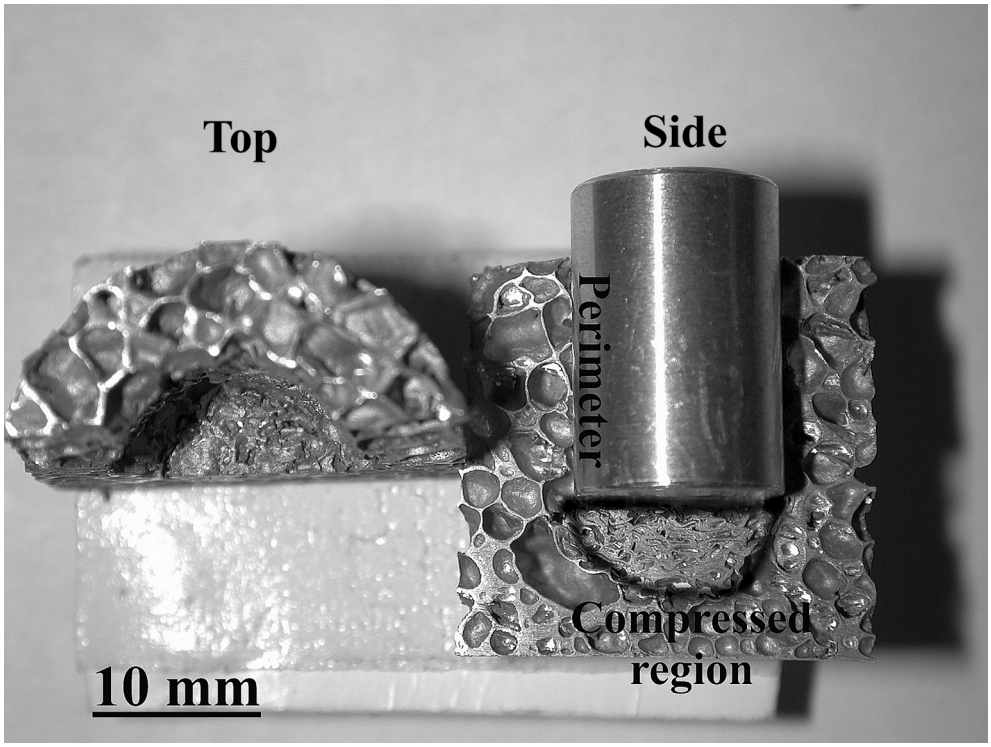

Figure 3.5 Cross-view (top and side) of an indented foam sample showing the compressed region under the indenter and the torn region around the indenter.

3.5 Energy Absorption

Foams can convert the much of the impact energy into plastic deformation energy and keep the peak force exerted on the object below the level, which causes damage. This characteristic is a potential for foams to be used as impact absorbers to protect people and fragile devices from impact.

Compared to bulk metals, foams absorb more energy at a constant load as shown in Figure 3.6 [40]. The energy absorption, W, is simply the area under the load-deformation curve up to certain length of L (Figure 3.6). Al foams are widely studied as filling materials for Al and steel tubes [2, 4, 41]. The results of these studies have shown that on specific energy base foam filled tubes absorb more energy than non-filled ones due to the interaction effect resulting from foam filling. Figure 3.7 clearly shows this effect: the force necessary to deform foam filled tube (F_{avg}) is bigger than some of the forces necessary to deform tube alone (F^0) and foam alone (F^F) [41]. Microscopic observations have also shown that foam-filled tubes form higher number of folds than empty tubes, which result in an increased energy absorption (Figure 3.8). The interaction effect has also been observed for the foam-filled tubes compressed in transverse direction. In this direction foam deforms also laterally and resists the crushing of the tube (Figure 3.9). One of the potential applications of foams as energy-absorbing filling materials is in car crash boxes inserted between bumper and chassis in order to reduce the extent of damage in the chassis upto the crash velocities of 15 km/h [23].

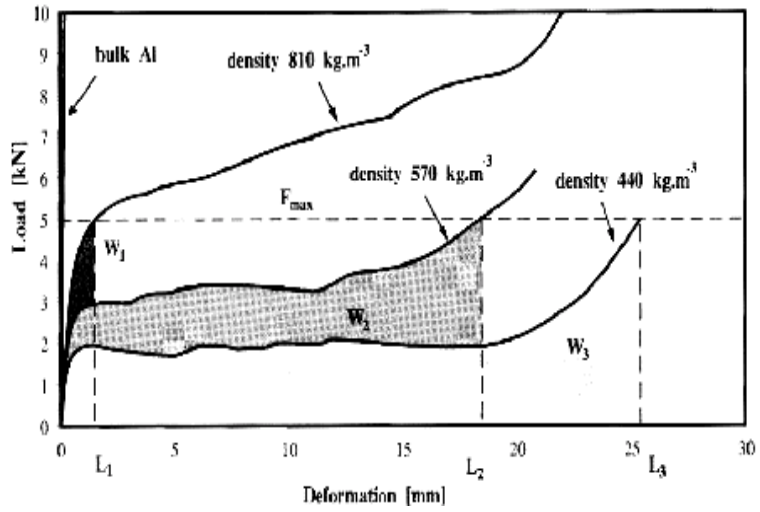

Figure 3.6 Comparison of energy absorption at constant loads between bulk metal and foams of different densities.

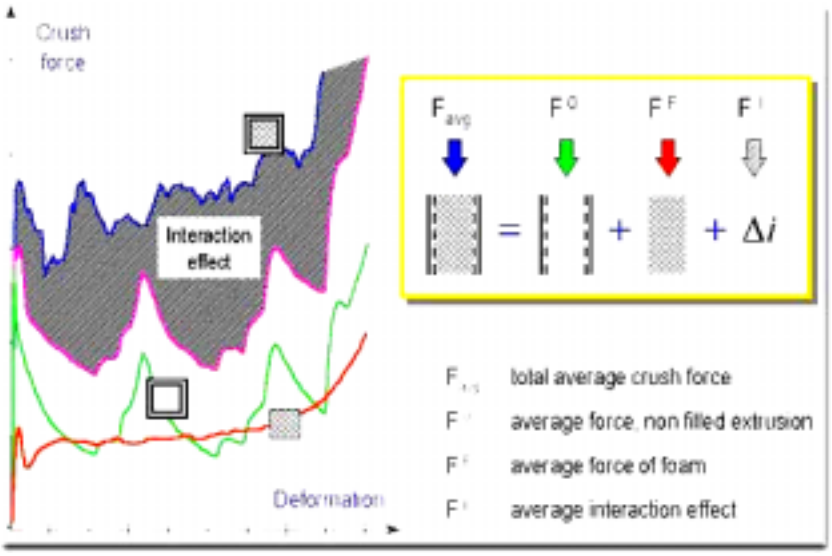

Figure 3.7 Compression force vs. deformation curves of foam, empty and foam filled tubes and interaction effect.

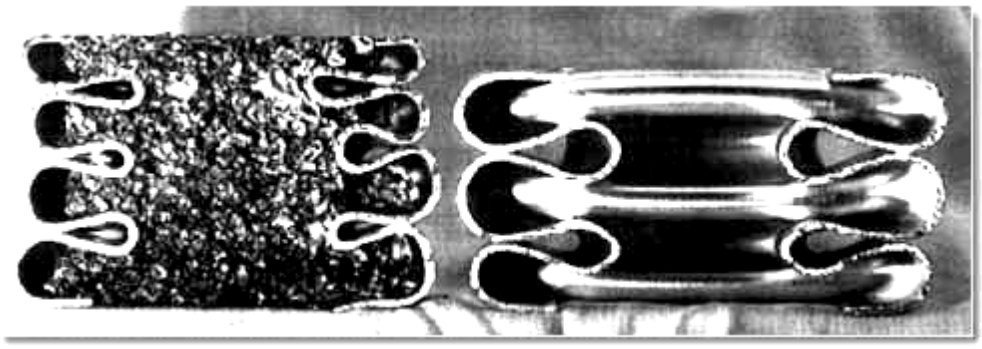

Figure 3.8 Micrographs of compressed foam-filled and empty tubes.

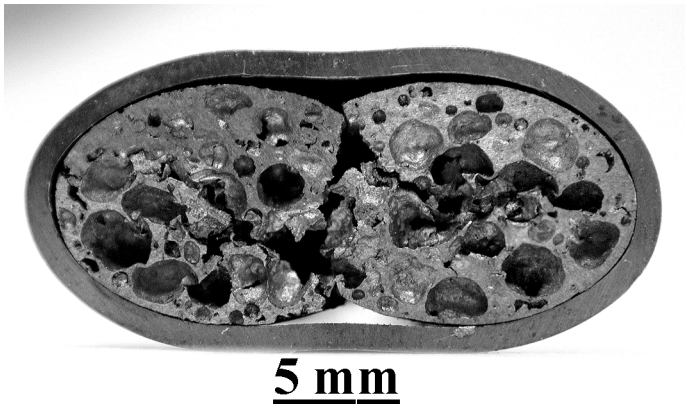

Figure 3.9 Micrograph of a transversely crushed foam-filled brass tube.

Chapter IV

EXPERIMENTAL

4.1 Materials

The specifications of materials (Al powder and granule, TiH_2 (blowing agent), SiC_p, Al_2O_{3p} and SiC_w) used to prepare foams are tabulated in Table 4.1. Pure Al was preferred to an alloy powder in order to avoid possible reactions between SiC_p and alloying elements, which may make the comparison between reinforced and unreinforced foams difficult. The main study on foaming and compression mechanical properties was conducted on 8.6 volume percentage (%) of SiC_p compacts and a few 20% SiC_p samples were also prepared and compression tested. Preliminary foaming experiments on Al_2O_{3p} and SiC_w/Al powder compacts were conducted as well. The content of blowing agent in all foaming experiments was chosen to be 0.5 wt.%, an amount found to be sufficient to form foaming in Al compacts [42].

The foam preparation method is schematically shown in Figure 4.1. The method consists of two major stages: a) preparation and b) foaming of powder compacts.

Table 4.1 Specification of raw materials

Material	***Size***	***Purity***
Al powder (Aldrich)	< 74 μm	99%
Al granule (Aldrich)	250-1680 μm	>99%
TiH_2 (Merck)	< 37 μm	>98%
SiC_p (Aldrich)	< 37 μm	
Al_2O_{3p} (Aldrich)	< 10 μm	99.7%
SiC_w (Tokai)	2-50 μm length, ~2 μm dia.	

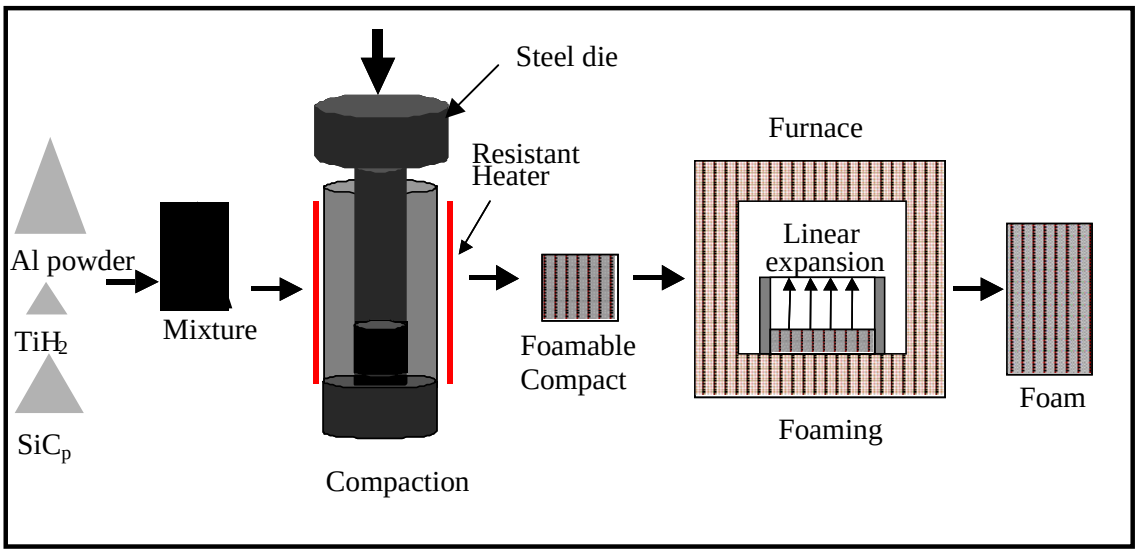

Figure 4.1 Schematic of foam preparation process.

4.2 Preparation of Powder Compacts

Appropriate amounts of basic ingredients were mixed inside a plastic container which was rotated on a rotary mill for 5 hours in order to form a homogeneous powder mixture. Compacts with a diameter of 27 mm and a thickness of ~9 mm were prepared from the powder mixture inside a steel die. Compaction was initially conducted at room temperature for a few minutes and followed by hot compaction at 425 ^{o}C for 1/2 hour. A resistant heater placed around the die was used to heat the die to the hot compaction temperature. The heating cycle, from room temperature to the compaction temperature, was one hour. The die pressure was kept constant at 220 MPa during cold and hot compactions and heating cycle.

4.3 Foaming of Powder Compacts

Foaming experiments were conducted in a preheated cubic furnace, Figure 4.1. Two foaming temperatures, 750 and 850 ^{o}C, higher than the melting temperature of Al, were selected and studied. The compacts were inserted into the furnace at room temperature inside a steel tube having the same diameter as the compact and a length of 8 cm. The steel tube was tightly closed at the bottom and placed vertically into the

furnace so that expansion was only limited to the vertical direction as designated by arrows in Figure 4.1. Inserting and removing specimen took less than 10 seconds. For each experiment furnace temperature was recorded and found to varying plus or minus 10 ^{o}C during foaming. Initial experiments were aimed at determining the effect of furnace holding time on the linear expansion of foam. Therefore, foamed or partially foamed material was taken from the furnace after a specified furnace holding time. These samples were either air cooled on a large steel plate or quenched by spraying water onto the steel tube holding the liquid foam. The heights of foam samples were measured in order to calculate linear expansion and then samples were cut through the longitudinal section by a diamond saw and metallographically prepared for microscopic observations.

4.4 Mechanical Testing

A second group of foams were prepared for the mechanical testing using the same process outlined above. In order to prepare foams of different densities, samples were taken from the furnace after various holding times. From these samples, cylindrical testing specimens, 20 mm in height and 20 mm in diameter, were core-drilled through the foam expansion direction. During core-drilling the pressure was kept as low as possible in order not to induce plastic deformation in the foam specimens. A typical compression sample prepared by core-drilling of the foamed sample is shown in Figure 4.2, together with the original foamed sample. Compression tests were conducted using an Instron testing apparatus at a cross-head speed of 0.1 mm s^{-1}. Tested foam samples were also metallographically prepared for microscopic observations of deformation mechanisms and for microhardness tests.

Figure 4.2 Cylindrical compression test sample (left) and the original foam specimen from which the test sample was core-drilled (right).

Chapter V

RESULTS AND DISCUSSION

5.1 Foaming Behavior of Al Powder and SiC_p/Al Compacts

The previous work on Al powder compaction for foamable compacts has indicated that maximum expansion was attained at compaction temperatures between 400 ^oC and 450 ^oC [42]. At lower compaction temperatures, hydrogen escaped through the interconnected porosity without expanding the compact during heating in the furnace [42]. For the present compacts, densities higher than 99% was only achieved at temperatures above 425 ^oC as shown in Figure 5.1. The compaction temperatures above 500 ^oC were found to be high enough to drive all the H_2 from the compact in the compaction stage, as will be elaborated below [42]. The relative density of the Al and 8.6% SiC_p/Al compacts prepared at 425 ^oC and under a pressure of 220 MPa was found to be 99%. Figures 5.2 (a) and (b) show the typical microstructures of the pure Al powder and composite compacts. These figures clearly show that no porosity existed in the compacts prepared using above parameters. Therefore, the chosen compaction temperature was an optimum temperature for the compaction pressure of 220 MPa.

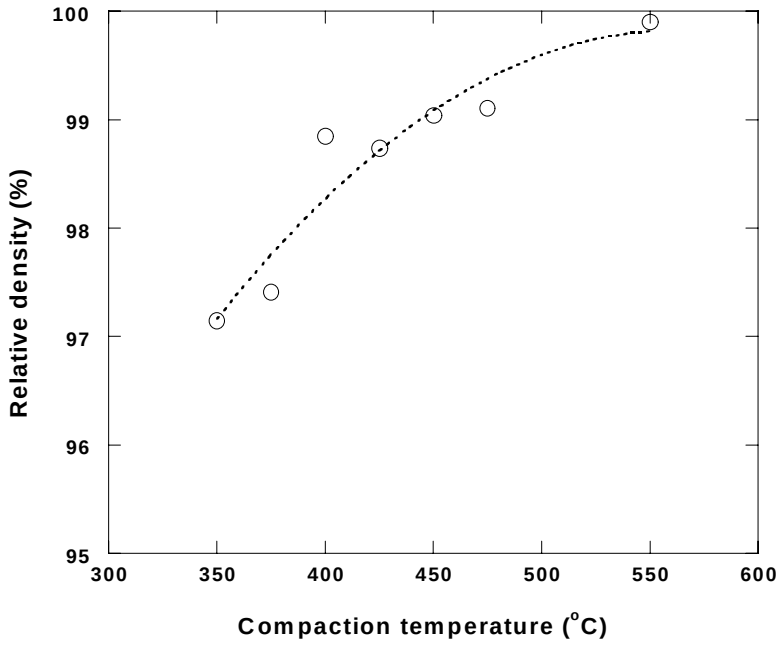

Figure 5.1 Relative density *vs.* compaction temperature for Al powder compacts.

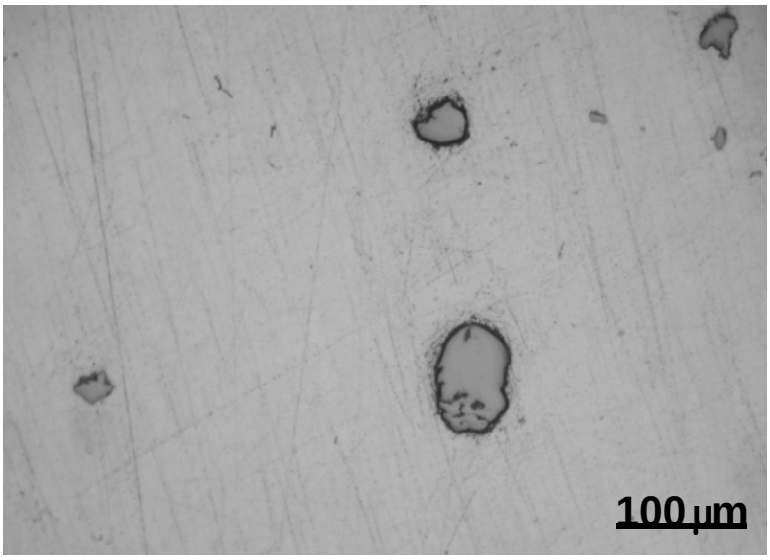

(a)

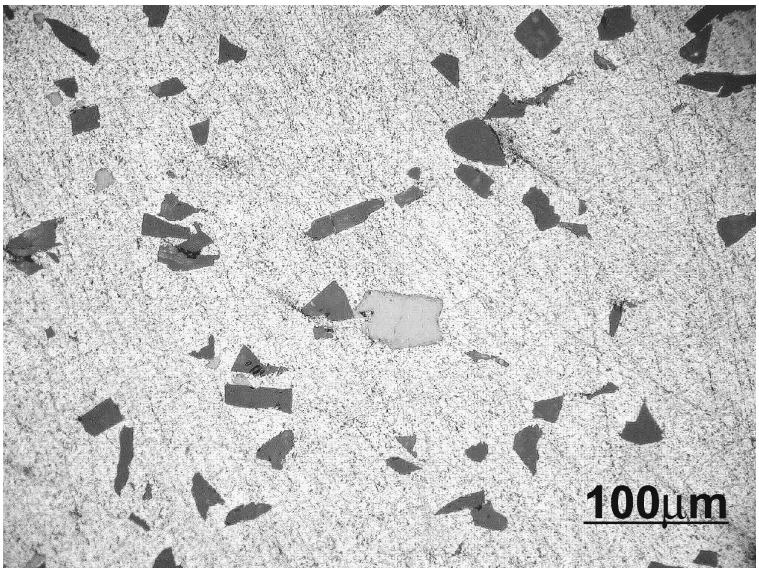

(b)

Figure 5.2 Optical micrographs of (a) Al and (b) SiC_p/Al compacts (gray particles are TiH_2 particles).

The effect of foaming temperature on the linear expansion (LE) of air-cooled foams is shown in Figure 5.3 for 750 and 850 ^oC. In Figure 5.3 and in the following figures, LE was calculated using,

$$LE = \frac{h_f - h_o}{h_o} \tag{5.1}$$

where h_f and h_o are the height of the foamed compact measured after a specific furnace holding time and initial compact, respectively. Foaming at both temperatures started after a certain furnace holding time, 5 minutes for 750 ^oC and 2-3 minutes for 850 ^oC (Figure 5.3). During this time, the compact was presumably being heated to some critical temperature before foaming started. The foam expansion increased rapidly until a maximum LE and then, with a small decrease, LE remained almost constant. Liquid foam samples taken from the furnace solidified within 20-30 seconds in air and underwent shrinkage during solidification. The increase of temperature from 750 to 850 ^oC, not affecting LE though, reduced the foaming time and the time to maximum LE.

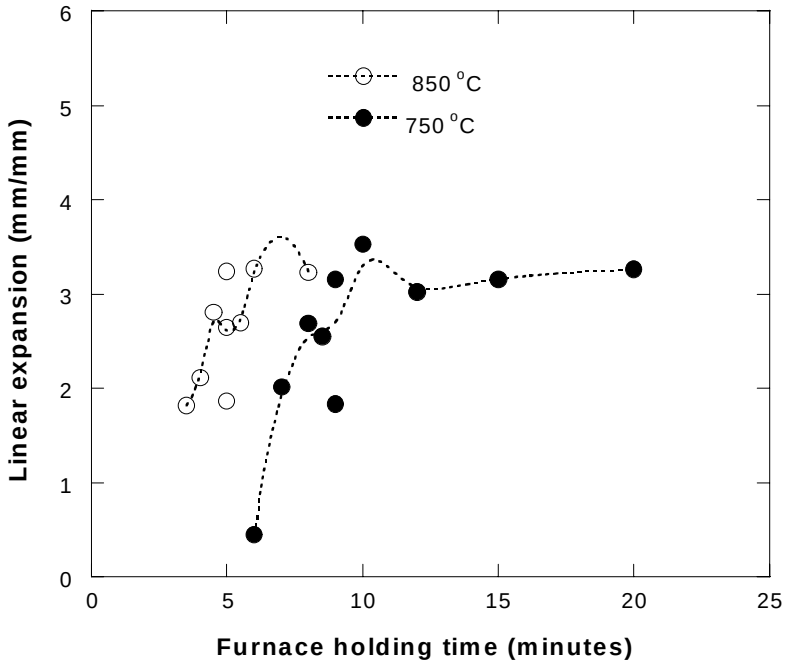

Figure 5.3 LE of Al compacts vs. furnace holding time at 850 and 750 ^oC pre-heating temperatures (air-cooling).

The rate of expansion of compacts during foaming was found to be affected by the pre-heated furnace temperature. A higher furnace temperature resulted in an earlier start of compact expansion (Figure 5.3). It is natural that, higher furnace temperatures would increase the heating rate of compacts in the furnace and may also reduce the viscosity of the liquid metal. For the investigated preheating temperatures, the compact foamed at 850 ^oC furnace temperature reached to the softening or melting point earlier;

therefore, expansion started earlier, 2-3 minutes, as compared with the compacts foamed at 750 ^{o}C (Figure 5.3). Although expansion was found to be earlier at 850 ^{o}C, the shape of the LE curve for both temperatures, 750 and 850 ^{o}C, did not alter significantly. A very similar measurement has been made in a study of foaming of Al-Si alloy [42]. It was proposed that after 750 ^{o}C, the expansion was saturated. Also the expansion of compacts at temperatures lower than 750 ^{o}C will be a subject for future studies. For the studied two furnace temperatures, 750 ^{o}C was identified as the temperature resulting more controlled foam expansion for the manufacture of different density foams.

Since air-cooling resulted in shrinkage of liquid foam after removal from the furnace, samples were quenched rapidly by spraying water on the steel cylinder holding liquid foam. Figure 5.4 shows both the effect of water quenching and SiC_p addition on the foaming of Al compacts. Water quenching yielded greatly increased LE of the pure Al composite foams, especially before the maximum LE. The SiC_p addition had two effects; it 1) increased the LE and 2) reduced the thickness of the dense Al layer at the bottom of the foam. Figure 5.5 shows structures of air-cooled pure Al and water quenched SiC_p Al foams at various furnace holding times. It is clearly seen from these

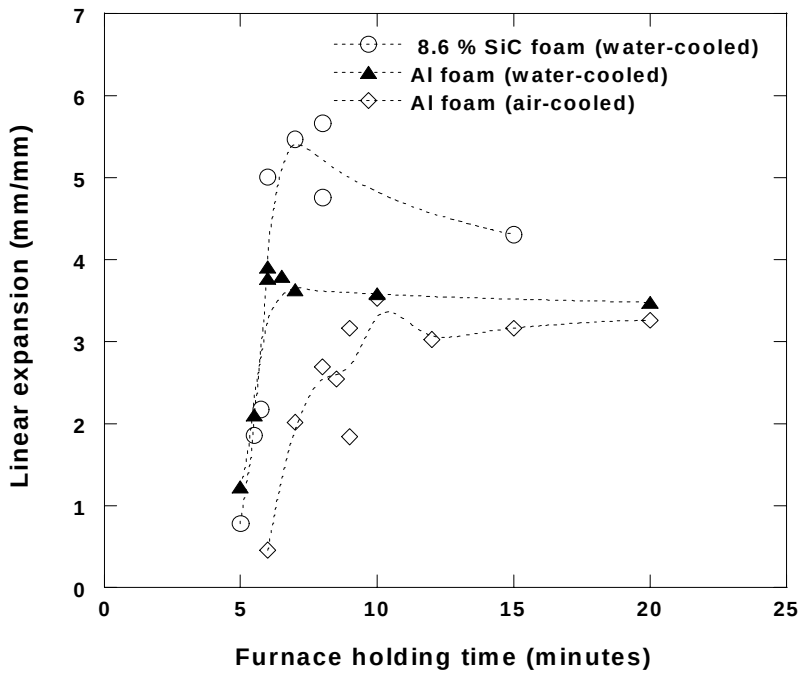

Figure 5.4 LE of Al and 8.6% SiC_p composite vs. furnace holding time at 750 ^{o}C pre-heating temperature.

figures that until a certain furnace holding time corresponding to maximum LE, expansion increased and from there with a slight decrease remained constant. Long furnace holding times resulted in collapse of the cells both on the top section and in the mid sections. Longer furnace holding times also increased the thickness of the dense Al layer at the bottom

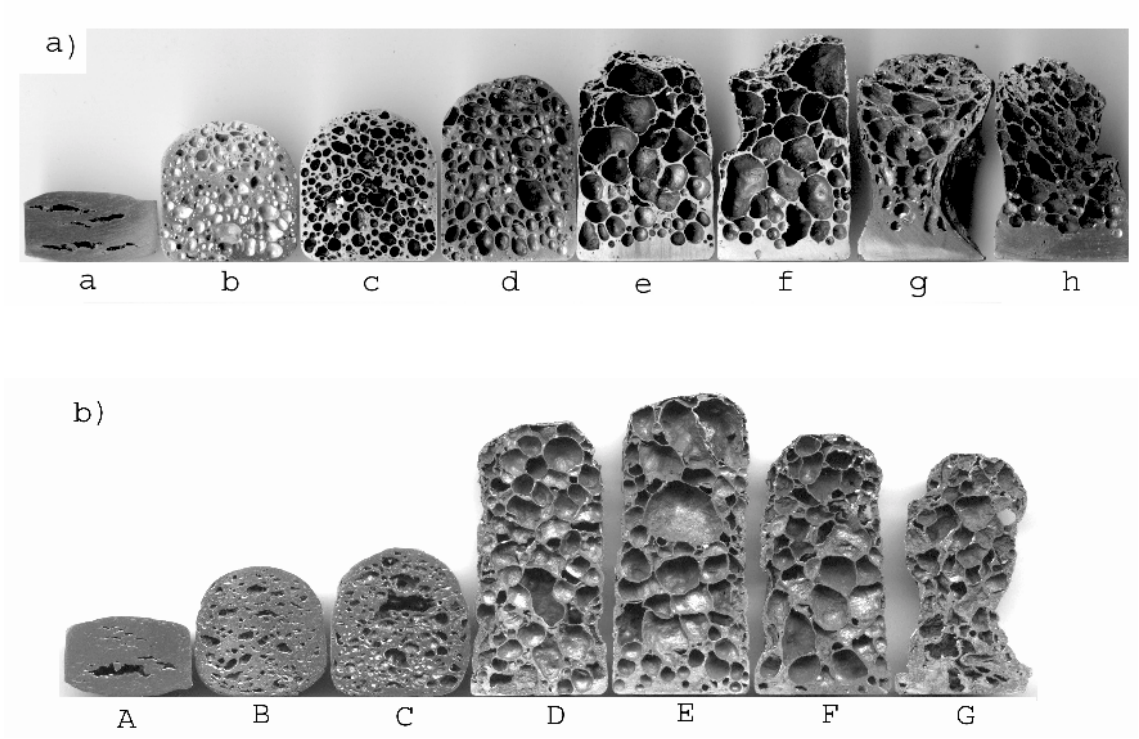

Figure 5.5 Foam structure evolution as a function of furnace holding time a) air-cooled Al compacts; a=6, b=6.45, c=7, d=8, e=9, f=10, g=15 and h=20 minutes b) water-cooled 8.6% SiC_p/Al compacts; A=5, B=5.30, C=5.45, D=6, E=7, F=8 and G=15 minutes.

Previous studies on TiH_2 have shown a decomposition process starting at 380 ^oC [9, 42]. The present hot compaction temperature was actually greater than the decomposition starting temperature of TiH_2; therefore, it is expected that some H_2 release would occur during compaction, before foaming in the furnace. This excess H_2 was claimed to be loosely bound and released at early stage of the foaming, leading a quick inflation of pores [42]. This accords well with the maximum LE observed in this study, which is probably a result of quick inflation of pores and release of some excess H_2 from the expanding foam. The foaming process is relatively fast, the partially melted/melted compact experienced a maximum LE within 1-2 minutes. Visual

observations had shown that some H_2 was released from the surface of the compact and burned in the furnace before foaming started.

Although foaming characteristics of the individual compacts prepared by the same processing parameters may alter depending on several factors such as spatial distribution of the blowing agent in each compact and so on, some generalizations could be made on the foaming sequence of the powder compacts based on Figures 5.5 (a) and (b). These are: 1) at the early stage of expansion pores were elongated normal to the compaction direction, a, A, B and C 2) initially elongated pores became more spherical in the later stages as the porosity increased, b, c, and d, 3) spherical pores were deformed into polyhedral shape before the maximum LE reached e, D and E, 4) Since no H_2 was released after maximum LE, foam decay started.

Foam decay occurs via two processes: coarsening and drainage [43]. Coarsening occurs due to the growth of the larger bubbles in the expense of smaller ones. This may be due to the pressure difference between two adjacent bubbles or simply due to the rupture of the cell wall of two adjacent bubbles. Drainage is the downward flow of the liquid metal through the cell edges due to gravitational forces. Drainage results in the formation of a thick dense layer of liquid metal at the bottom and cells with thicker walls in the middle. Particulate addition to the foams is known to have a stabilizing effect. The presence of particles on the cell walls increases the viscosity of the liquid; therefore, reduces the liquid metal flow [44]. This effect was clearly seen in Figure 5.5.

It was also found in this study that, the liquid foam must be cooled rapidly in order to retain the liquid cell structure in the solid state, otherwise collapse of the cells occurs particularly at the upper part where the buoyancy effects tend to destroy the bubbles. The lateral contractions observed at longer holding times in Figure 5.5 (a) and (b) are also due to this effect; bubbles rise and cannot be replaced once the TiH_2 has been completely consumed, leading to a contraction and an increase in thickness of the Al skin at the cylinder base. Although liquid foam was quenched by spraying water on the steel tube holding foam, in industrial applications molds could be designed with water circulation.

5.2 Foaming Behavior of Al Granule, Al_2O_{3p}/Al and SiC_w/Al compacts

Initial foaming experiments (750 ^oC) on 8.6% Al_2O_{3p}/Al compacts prepared using the same process parameters resulted in LE's similar to those of Al compacts. A

higher number of irregular cells and a more inhomogeneous cell size distribution were also observed in these foams (Figure 5.6 (a) and (b)). The foaming attempts of 8.6% SiC_w/Al compacts were not successful and it was presumed that the chosen compaction temperature and pressure combination was not enough to form a gas-tight structure in these compacts.

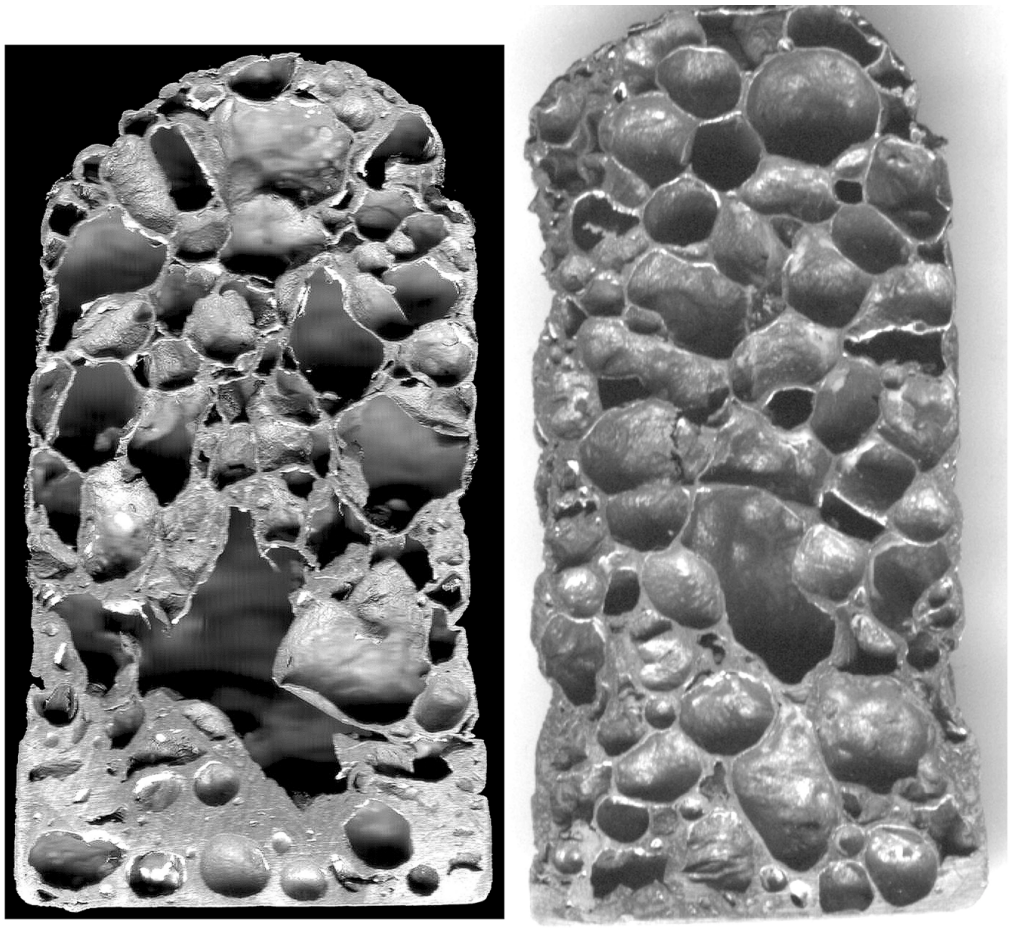

Figure 5.6 Micrographs of a) 8.6% Al_2O_{3p}/Al and b) 8.6% SiC_p/Al composite foams cell structures.

Al granules were also used to prepare compacts using the same process parameters. This is mainly due to the lower cost of the granules as compared with the powders. However, the LE in granule compacts were found to be less than 2, which was significantly lower than that of powder compacts (4-5). This might be partly because due to the large size differences between blowing agent and the granules, which

probably resulted in an inhomogeneous distribution of the blowing powder and the applied compaction pressure which might not be sufficient to produce a gas-tight compact. It was also observed that H_2 in the SiC_w/Al compacts left the system prior to the melting/softening point of the compacts. A detailed experimental study on granule and compacts will be conducted in the future. However, this showed the importance of the selection of an optimum powder size-compaction pressure combination which will result in a homogeneous distribution of powders and a gas-tight compact density.

5.3 Compression Behavior of Al and SiC_p/Al Foams

Figures 5.7 (a), (b) and (c) show the effect of foam density on the compressive stress-strain behavior of Al and SiC_p/Al composite foams, respectively. The stress levels for the SiC_p/Al composite foam is higher than that of Al foam for the same foam density as shown in Fig. 5.8 (a) and (b). This stress level difference became smaller with deformation and at large strain levels (about 0.8) both samples had a similar compressive stress-strain behavior (Figure 5.8 (a)).

Compression mechanical behavior of Al closed-cell foams has been recently reviewed by Gibson and it was shown that most of the commercially available Al closed-cell foams behave similarly with the open cell foams [45]. During compression thinner cell walls buckle and cell edges crush over the cell walls which was stated in Chapter 3. Although detailed observations on morphological features of the prepared foams and tested foams will be conducted in another study, preliminary observations on undeformed and deformed samples have confirmed that the investigated composite and Al foams have similar cell morphology and deformation characteristics with commercially available Al closed-cell foams. These are; (1) cell edges are thicker than the cell walls (Figure 5.9), (2) during compression cell walls buckle and as a result of this cell edges crush over the cell walls (Figure 5.10) and (3) cell walls also fail due to the lateral tensile strains.

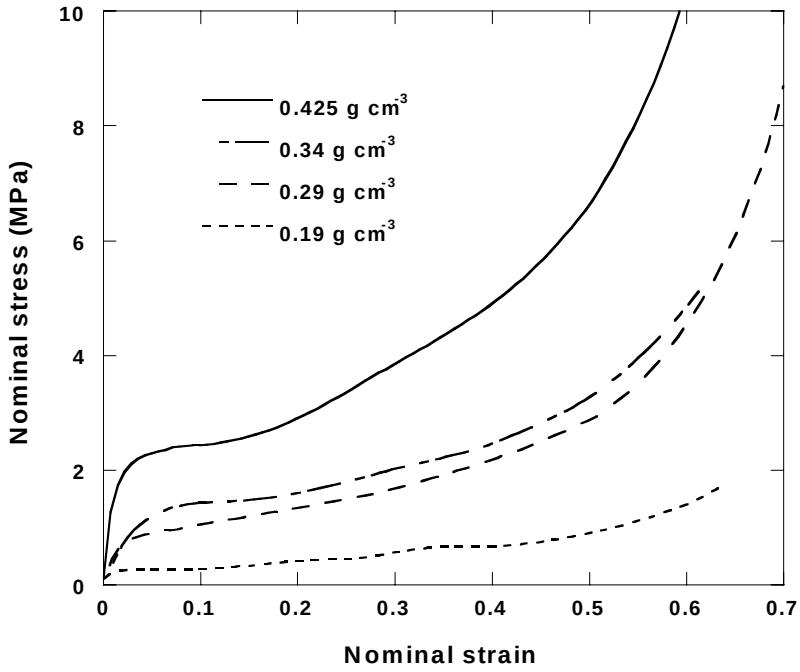
Nominal stress (MPa)
Nominal strain
0.425 g cm-3
0.34 g cm-3
0.29 g cm-3
0.19 g cm-3
0
2
4
6
8
10
0
0.1
0.2
0.3
0.4
0.5
0.6
0.7

(a)

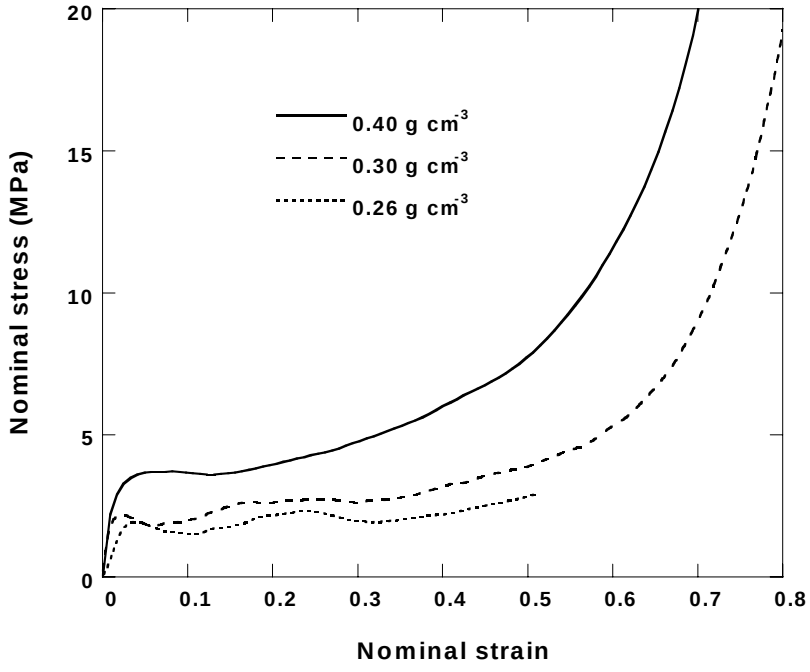
Nominal stress (MPa)
Nominal strain
0.40 g cm-3
0.30 g cm-3
0.26 g cm-3
0
5
10
15
20
0
0.1
0.2
0.3
0.4
0.5
0.6
0.7
0.8

(b)

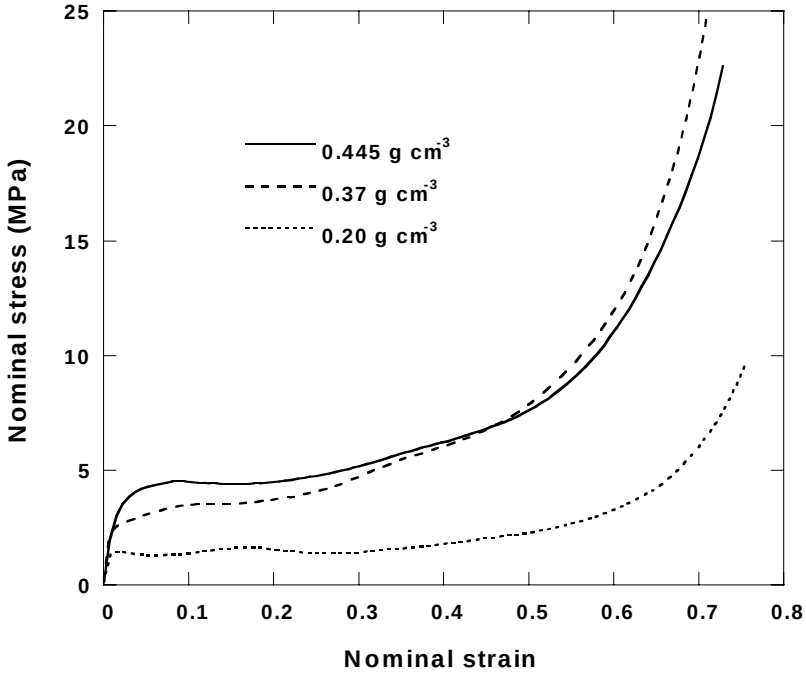

(c)

Figure 5.7 Compression stress-strain curves of (a) Al, (b) 8.6% SiC_p and (c) 20% SiC_p composite foams at various densities.

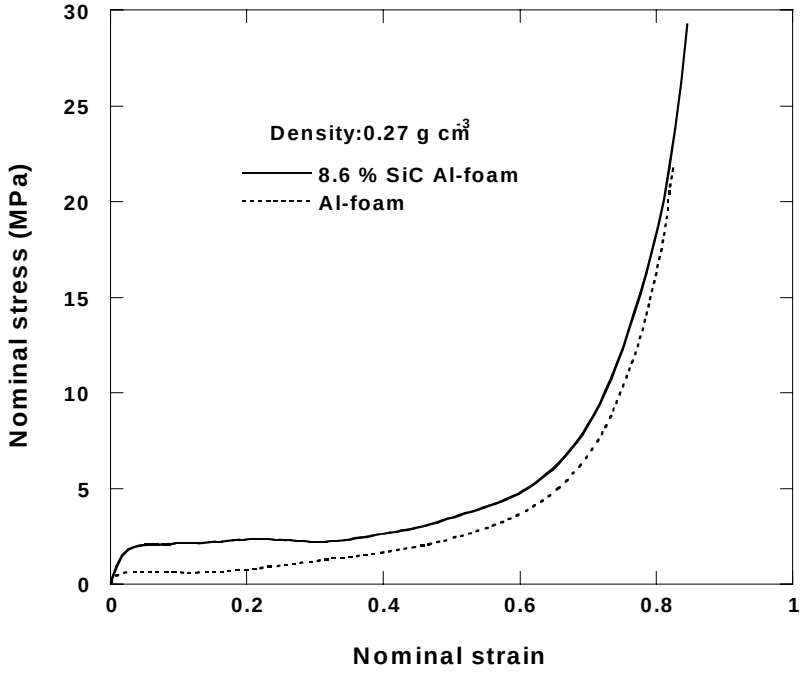

(a)

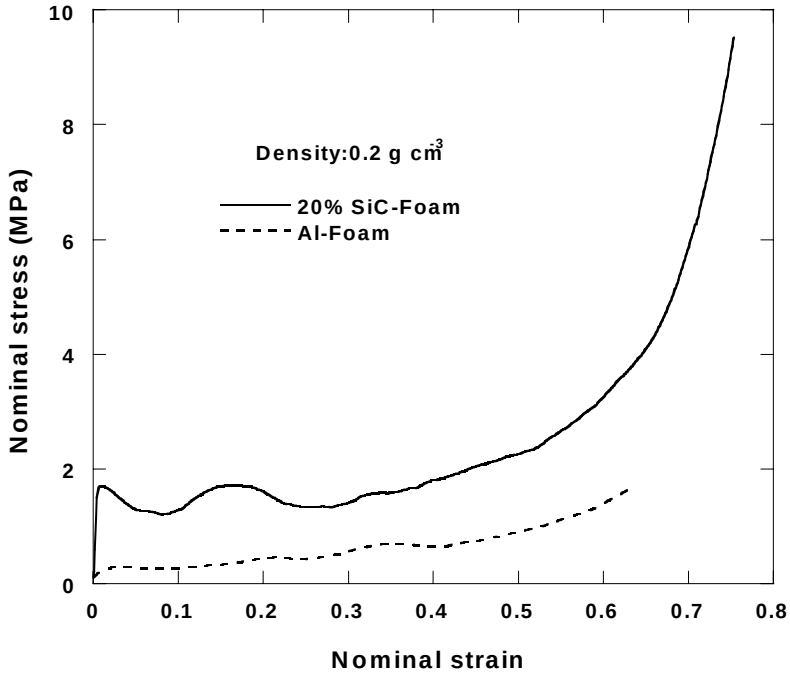

(b)

Figure 5.8 Compression stress-strain curves of (a) Al and 8.6% SiC_p composite and (b) Al and 20% SiC_p composite foams at similar densities.

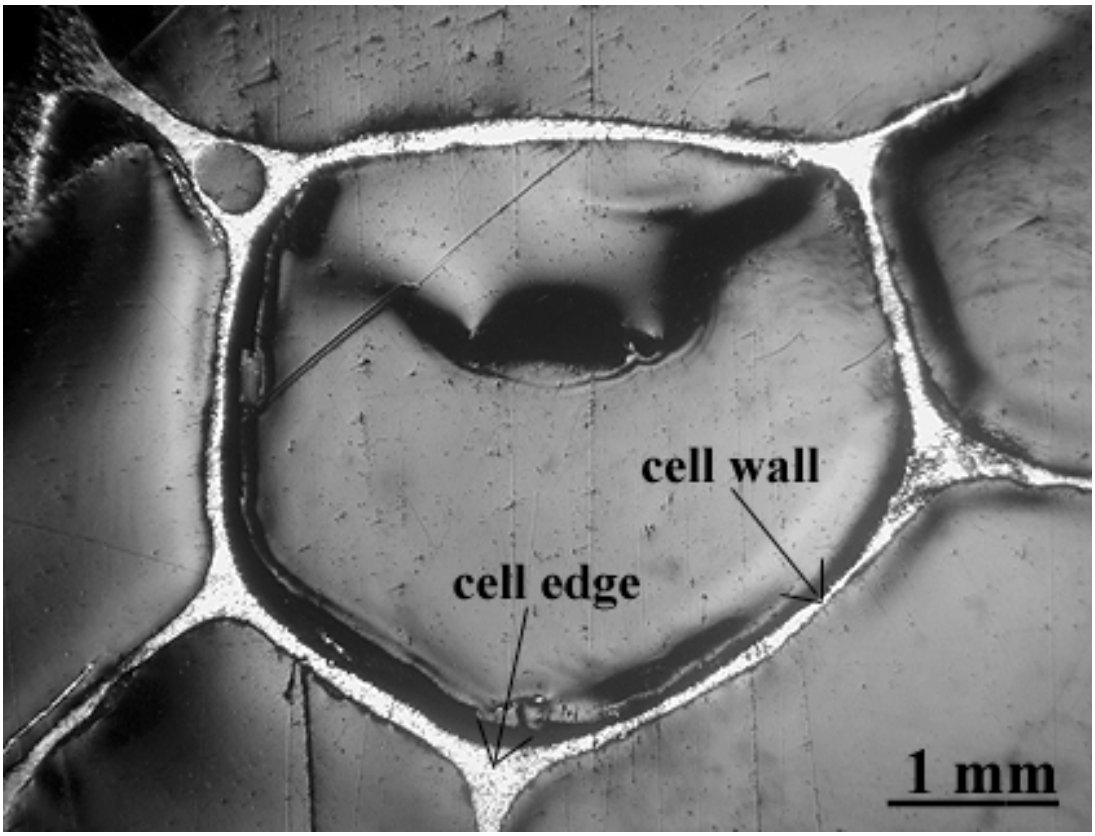

Figure 5.9 Optical micrograph of 8.6% SiC_p/Al foam cell structure.

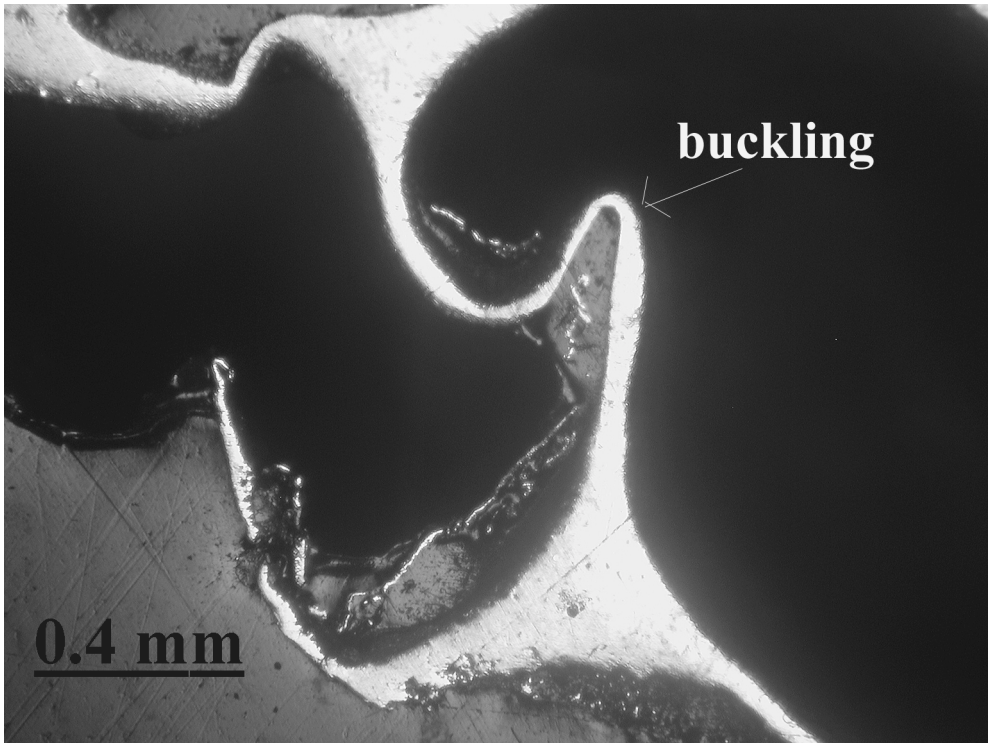

Figure 5.10 Optical micrograph of 8.6% SiC_p/Al foam, showing cell wall buckling.

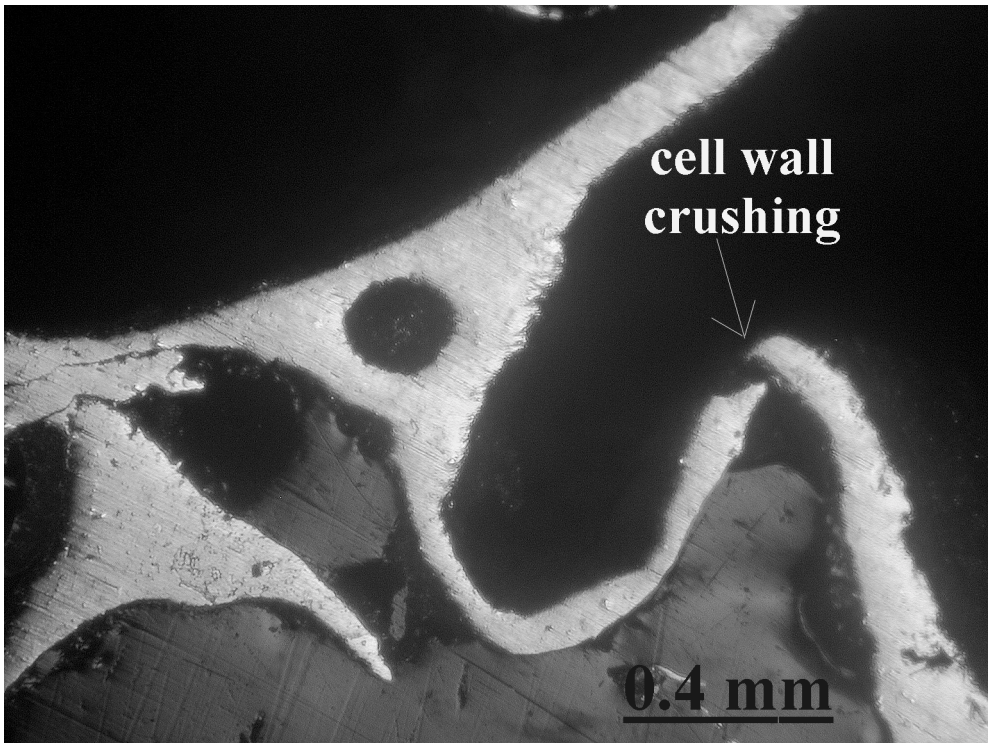

Figure 5.11 Optical micrograph of 8.6% SiC_p/Al foam, showing cell wall buckling and crushing.

The collapse stress or plateau stress of the present foams based on above observations, was fitted to the following equation:

$$\sigma^*_{pl} = \sigma_{ys} C(\rho)^{3/2} \tag{5.2}$$

which was developed for open cell foams [1]. Data for a wide range of Al foams suggested that C~0.3 [13]. The relative density of the composite was determined by the rule of mixtures (2.7 g cm^{-3} for Al and 3.23 g cm^{-3} for SiC_p). Experimental data of Al and composite foams were well fitted to Equation 5.2 (Figure 5.12). The values of σ_{ys} in Equation 5.2 were predicted as 230 and 100 MPa for composite and Al foams respectively, which shows that the plateau stress of the composite is about two times higher than that of the Al foam.

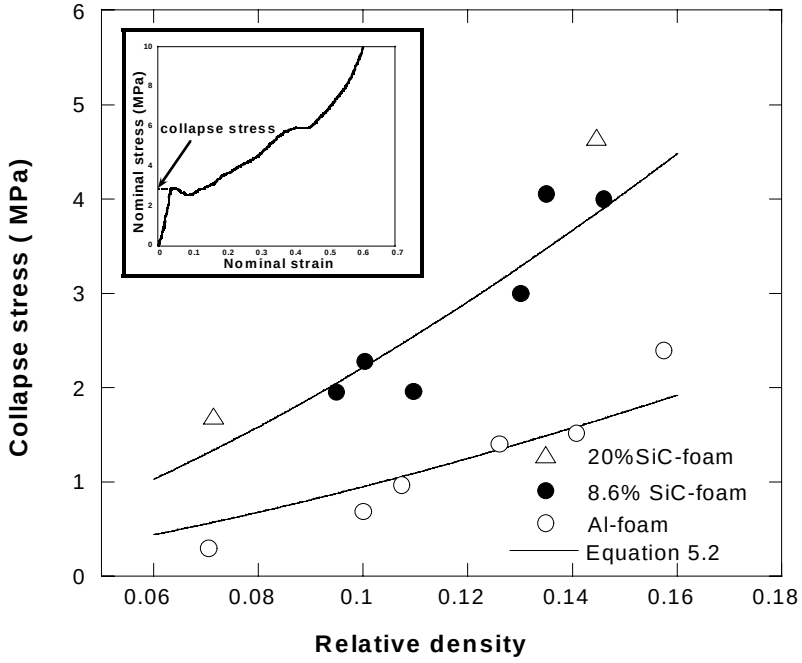

Figure 5.12 Variation of collapse stress with relative density.

Microhardness (Vickers) measurements were used to estimate the σ_{ys} in Al foam using [46],

$$\sigma_{ys} = \frac{HV}{3} \tag{5.3}$$

where HV is the Vickers Hardness. Estimated average σ_{ys} values were 90 MPa and 80 MPa on the cell wall and cell edge, respectively. These results are very similar to the σ_{ys} value (100 MPa) predicted using Equation 5.2. The σ_{ys} difference between cell edge and cell wall may be partly due to the preferential formation of hard compounds on the cell walls such as Al-Ti intermetallic compound.

Presence of hard ceramic particles generally increases the flow stress of a metal matrix. In SiC_p/Al composite, the possible contribution to the MMCs strength might be the load transfer to the particles (σ_p), internal stresses, subgrain size, enhanced dislocation density due to coefficient of thermal expansion (CTE) difference and geometrically necessary dislocations (GNDs).

The load transfer due to the particles can be estimated using the following equation [47],

$$\sigma_p = \sigma_{um}(\frac{1}{2}V_p(s+2) + V_m) \quad (5.4)$$

where σ_{um}, V_p and V_m are unreinforced matrix strength, particle and matrix volume fractions, respectively and s is the aspect ratio of particles (length/radius). The aspect ratio of SiC_p is predicted from Figure 5.13 (a) and (b), which shows the particle distribution and the particle alignment on cell edge and cell wall of a 8.6% SiC_p/Al composite foam. The vertical direction in these micrographs show the foam expansion direction; therefore the compression axis. As clearly seen in this micrograph, the particles are irregular in shape and the longer axis of the particles are aligned through the compression direction especially on the cell wall. Therefore, an aspect ratio of 4 was estimated based on the above observations. The contribution of the particles on the strength of the composite (σ_p-σ_{um}) is calculated to be only 20 MPa using equation 5.4.

The difference in the coefficient of thermal expansion between matrix and fiber almost unavoidably results in internal stresses as the composite cools down from the elevated production temperature. Part of these stresses is relieved by the generation of dislocations and the remaining misfit gives rise to a build-up of tensile residual stresses in the matrix. Dislocations generated upon cooling increase the strength of the composite by the following equation [47],

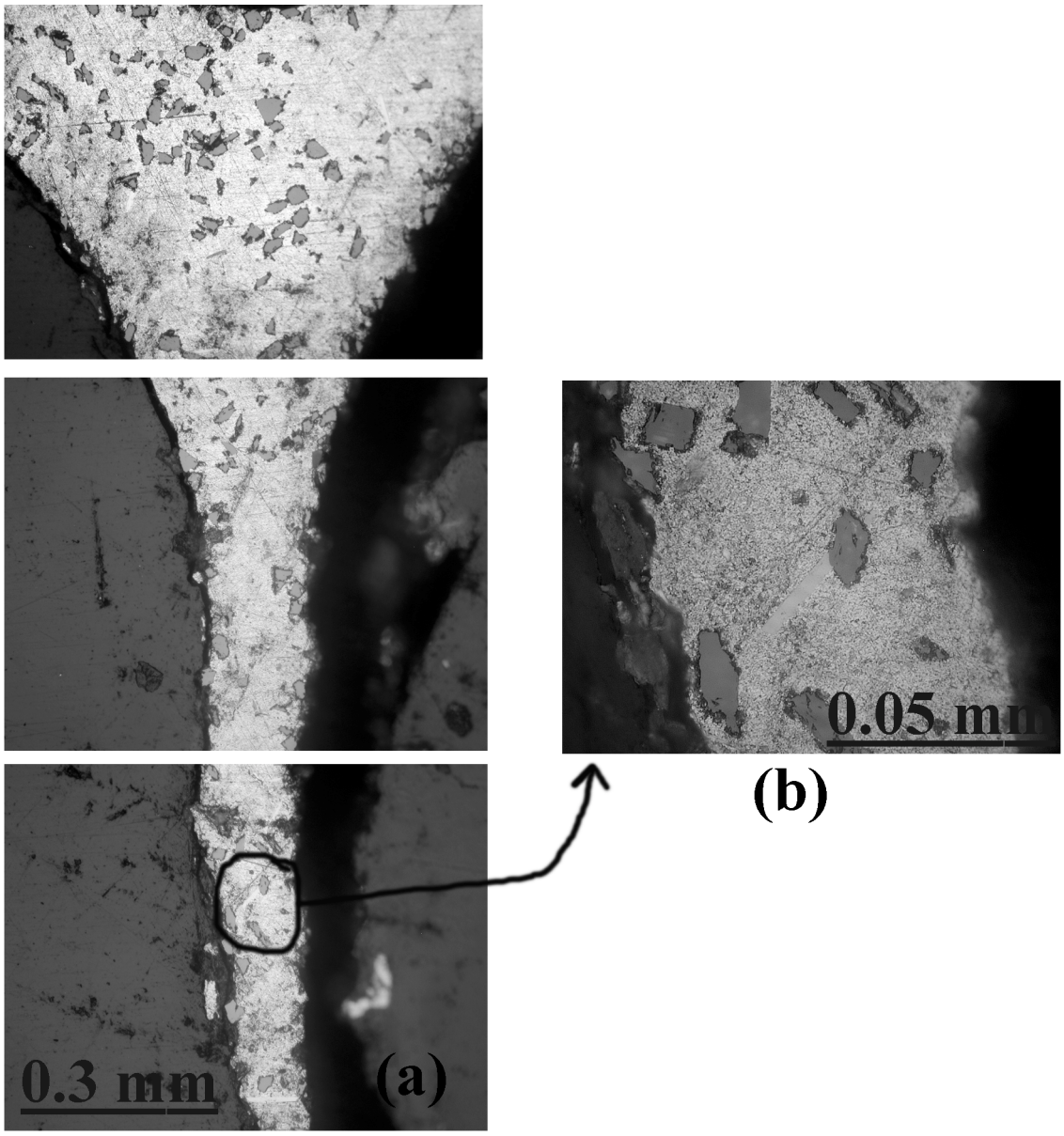

Figure 5.13 Optical micrographs of SiC_p distribution on a) cell edge and cell wall and b) particle alignment through the foam expansion and compression axes on the cell wall of 8.6 % SiC_p composite foam.

$$\Delta\sigma_{Dis} = \alpha G b \sqrt{\rho} \tag{5.5}$$

where $\Delta\sigma_{Dis}$ is the strengthening due to dislocations, α is a constant, G is the shear modulus and b and ρ are the Burger's vector and dislocation density, respectively. The dislocation density generated by thermal cooling was formulated by Humphreys [48] for

a dispersion of cubic particles of side L. The dislocation density is calculated by assuming that all the thermal stresses are relieved by dislocation generation and is given as

$$\rho = 12V_p \Delta(CTE)\frac{\Delta T}{bL} \tag{5.6}$$

where Δ(CTE) and ΔT are the difference in thermal expansion coefficients of the phases and the temperature change respectively. For the considered composite structure using following values; V_p~0.1, Δ(CTE)=19.6x10^{-6} K^{-1} [49], ΔT= 700 K, L~10x10^{-6} m, α=1.25 [50], G= 2.64x10^4 MPa, b= 2.86x10^{-10} m and Equation 5.5 and 5.6 the increased matrix strength is estimated to be about 20 MPa.

The MMCs usually have finer grain size as compared to monolithic alloys. The typical grain sizes in particulate reinforced MMCs are around 10 μm [49]. The strengthening due to grain size refinement in composite can be determined using the Hall-Petch equation

$$\Delta\sigma_G = k_y d_g^{-\frac{1}{2}} \tag{5.7}$$

where k_y is a constant and d_g is the grain size. For example for a 10 μm. grain size with k_y= 0.1 MPa $m^{-1/2}$ [48], the grain size strengthening would be as high as 30 MPa.

Note that the predicted composite yield strength (230 MPa) using Equation 5.2 is still higher than the sum of contributions of several effects explained above. For a similar composite (15% SiC_p/2024 Al) and a matrix alloy with a yield stress of ~100 MPa, an increase in compression yield stress as high as 100 MPa was found experimentally [51].

It has also been found that the cell morphology such as cell wall and cell edge thickness have affected the plateau stress. For the present foam both, increase of yield stress of the foaming material and change of cell morphology, due to presence of SiC_p, may be effective in the increase of plateau stress of the composite foam as compared to the Al foam. These effects will be studied in detail in a further project, which will focus on yield stresses of the foaming materials and effect of SiC_p on the foam cell morphology.

The energy absorption per unit volume (E) will be the area under the stress-strain curve and is explained as,

$$E = \int_0^{\varepsilon^*} \sigma \, d\varepsilon \tag{5.8}$$

where ε^* is the limit strain for which the energy absorption is considered. For the present foams, as a comparison for energy absorption differences between composite and Al foams, energy absorption capabilities as function of relative strain are shown in Figure 5.14 for the limit strains of 10 and 30%. Figure 5.14 clearly shows that composite foams provides more energy absorption than Al foams.

Present study has shown that the plateau stress; therefore the energy absorption capability of Al foams can be increased greatly by the SiC_p incorporation. Foams with different energy absorption capacities can be tailored by varying the content, size and even the shape of the particles without increasing the density of the foam. Preliminary results of increasing content of SiC_p has resulted in an increase in plateau stress as shown in Figure 5.12 and proven the potential for higher plateau stresses.

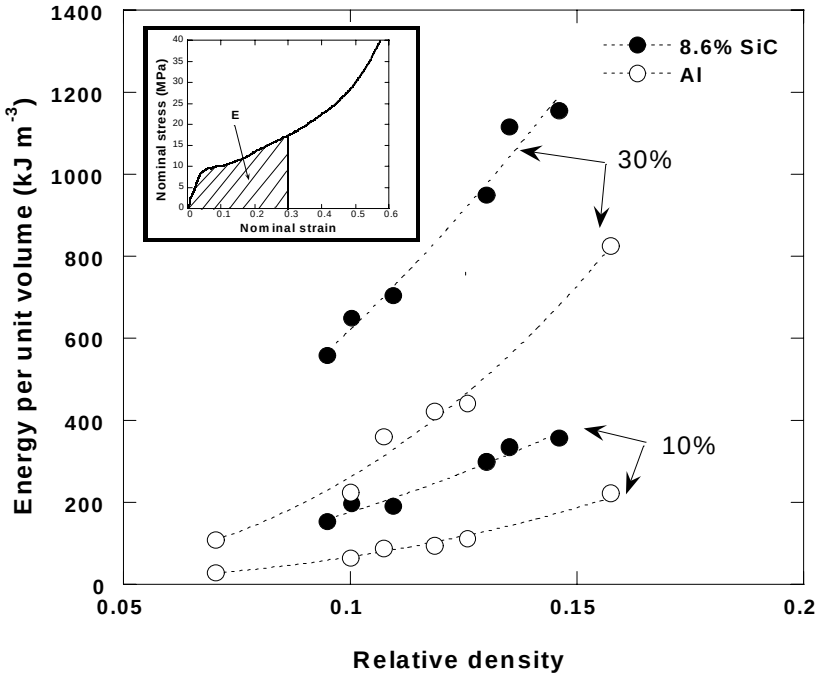

Figure 5.14 Energy absorption vs. relative density of Al and 8.6% SiC_p composite at 10 and 30% strains.

Chapter VI

CONCLUSIONS

Foaming and compression mechanical behavior of SiC_p/Al composite powder compacts and foams prepared by the foaming from powder compact process were determined and compared with those of pure Al compacts and foams prepared by the same processing parameters in order to assess the effect of SiC_p addition on foaming and mechanical properties.

Initial foaming experiments with Al compacts at 750 and 850 ^oC have shown that foaming at the former temperature was slower and more controllable, although LE was similar at both temperatures. Rapid cooling of the foamed liquid metal was also found to be necessary in order to maintain the liquid foam structure in the solid state.

Foaming experiments of SiC_p/Al and Al compacts at 750 ^oC have shown that SiC_p addition a) increased LE of the powder compacts and b) reduced the extent of liquid metal drainage. SiC_p addition also increased the plateau stress and the energy absorption. These results have shown that the potential of composite foams for tailoring energy absorption of aluminum foams for varying levels of impact stresses.

Foaming experiments on Al_2O_{3p}/Al composite compacts resulted in no significant increase in LE as compared to Al compacts, showing the inefficiency of these particles in foaming of the Al compacts. In SiC_w/Al composite compacts no expansion was observed, which might be due to the insufficient compaction temperature-pressure combination for a fully dense compact preparation.

REFERENCES

1. L. J. Gibson and M. F. Ashby, "Cellular solids: structures and properties", Cambridge University Press, 1997.

2. M. Seitzberger, F. G. Rammerstorfer, and H. P. Degischer, "Crushing of axially compressed steel tubes filled with aluminum foam", Acta Mechanica, 125 (1997) 93-105.

3. A. G. Hanssen, M. Langseth, O. S. Hopperstad, Int. J. Solids and Structures 24 (2000) 475.

4. I. W. Hall, Ö. Ebil, M. Güden and C.-J. Yu, "Quasi-static and dynamic crushing of empty and foam-filled tubes", J. Mater. Scie., in press.

5. A. G. Evans, J. W. Hutchinson, M. F. Ashby, "Multifunctionality of cellular metal systems", Prog. Mater. Sci., 43 (1999) 171-121.

6. A. E. Simone and L. J. Gibson, "The effects of cell face curvature and corrugations on the stiffness and strength of metallic foams", Acta mater., 46 (1998) 3929-3935.

7. R. Gradinger, F. G. Rammerstorfer, "On the influence of meso-inhomogeneties on the crush worthiness of metal foams", Acta Mater., 47 (1999) 143-148.

8. T. Miyoshi, M. Itoh, T. Mukai, H. Kanahashi, H. Kohzu, S. Tanabe, K. Higashi, "Enhancement of energy absorption in a closed-cell aluminum by the modification of cellular structures", Scripta Mater., 41 (1999) 1055-1060.

9. F. Baumgartner, I. Duarte, J. Banhart, "Industrialization of powder compact foaming process", Advanced Eng. Mater., 2 (2000) 168-174.

10. Wood, J. T., "Production and applications of continuously cast foamed aluminum", Fraunhofer USA Metal Foam Symposium, J. Banhart and H. Eifert Edn. Stanton, Delaware, 7-8 Oct. 1997.

11. US Patent, 4973358

12. L. J. Gibson and A. E. Simone, "Aluminum foams: structure and properties", Mechanics and materials seminar, 3 April, 1997.

13. O. Prakash, H. Sang, J. D. Embury, "Structure and properties of Al-Si foam", Mater. Sci. Eng., A199 (1995) 195-203,.

14. T. Miyoshi, M. Itoh, S. Akiyama, A. Kitahara, "Alporas aluminum foam: production process, properties, and applications", Adv. Eng. Mater., 2 (2000) No:4 179-183.

15. J. Banhart, "Metallic foams: challenges and opportunities", Eurofoam 2000, MIT-Verlag Bremen, 2000, 13-20.

16. J. Banhart, "Production Methods for Metallic Foams", Fraunhofer USA, Metal Foam Symposium, Symposium Proceedings, Delaware, Oct. 7-8, 1997, Verlag Pub. Bremen, 1998.

17. US Patent, 5151246

18. C. Yu, H. Eifert, J. Banhart, J. Baumeister, "Metal foaming by a metallurgy method: production, properties and applications", Journal of Materials Research Innovations, 2 (3) 1998.

19. "Metal foams near commercialization", Metal Powder Report, April, (1997) 38-41.

20. J. Banhart, "Manufacturing routes for metallic foams", JOM, 52 (12) (2000), 22-27

21. V. Gergely and B. Clyne, “The Formgrip process: foaming of reinforced metals by gas release in precursors”, Adv. Eng. Mater., 2 (2000) No:4 175-178.

22. Anne-Marie Harte, Norman A. Fleck, M. F. Ashby, "Sandwich panel design using aluminum alloy foam", Adv. Eng. Mater., 2 (2000) No:4 219-222.

23. A. Fuganti, L. Lorenzi, A. G. Hanssen and M. Langseth, ”Aluminum foam for automobile applications”, Advan. Eng. Mater., 2(2000)200-204.

24. U. Galovsky, R. Kretz, " Manufacturing of large size aluminum foam netshape parts for automotive applications", ISATA-Wien, 14.-16 June (1999).

25. J. Banhart, "Properties and applications of cast aluminum sponges", Advan. Eng. Mater., 2 (2000) 188-191.

26. M. Güden, I. W. Hall, C. -J. Yu, "Quasi-static and dynamic crushing of an aluminum closed-cell foam", TMS Meeting, 1998.

27. I. W. Hall, M. Güden and Yu, "Crushing of aluminum closed-cell foams: density and strain rate effects", Scrpt. Mater., 43 (2000) 515-521.

1. S. Elbir, S. Yılmaz, M. Güden, "Kapalı hücreli alüminyum köpük metallerin üretim metotları ve mekanik özellikleri", Metalurji Dergisi, 120 (1999) 35-42.

29. A. E. Simone, L. J. Gibson, "Effect of solid distribution on the stiffness and strength of metallic foams", Acta Mater., 46(1998) 2139-2150.

30. S. K. Maiti, L. J. Gibson and M. F. Ashby, "Deformation and energy absorption diagrams for cellular solids", Acta mater., 32(1984) 1963-1975.

31. M. Ashby. A. G. Evans, N. A. Fleck, L. J. Gibson, J.W. Hutchinson and H. N. G. Wadley, "Metal foams design guide", Cambridge, 1999.

32. K. Y. G. McCullough, N. A. Fleck and M. F. Ashby, "Uniaxial stress-strain behavior of aluminum alloy foams", Acta Mater. 47(1999) 2323-2330.

33. C-J. Yu and J. Banhart, "Mechanical properties of metallic foams", Fraunhofer USA Metal Foam Symposium, J. Banhart and H. Eifert Edn. Stanton, Delaware, 7-8 Oct. 1997.

34. J. T. Beals and M. S. Thompson, "Density gradient effects on aluminum foam compression behavior", J. Mater. Scie., 32(1997) 3595-3600.

35. Y. Sugimura, J. Meyer, M. Y. He, H. Bart-Smith, J. Grenstedt and A. G. Evans, "On the mechanical performance of closed cell Al alloy foams", Acta Mater.,12(1997)5245-5259.

36. J. L. Grenestedt, "Influence of imperfections on effective properties of cellular solids", MRS Symposium Proceedings Vol.521, San Francisco, 1998.

37. J. Banhart and J. Baumeister, "Deformation characteristics of metal foams", J. mater. Scie. 33(1998) 1431-1440.

38. M. Güden and I. W. Hall, unpublished work.

39. O. B. Olurin, N. A. Fleck and M. F. Ashby, "Indentation resistance of an aluminum foam", Scripta Mater., 43(2000) 983-989.

40. Facts & Data, Alulight.

41. A. G. Hanssen, M. Langseth and O. S. Hopperstad, "Static and dynamic crushing of square aluminum extrusions with aluminum foam filler", Int. J. Impact Eng., 24(2000) 347-383.

42. I. Duarte, J. Banhart, "A study of aluminum foam formation-kinetics and microstructure", Acta Mater., 48 (2000) 2349-2362.

43. S. Cox, G. Bradley, and D. Weaire, "Modelling metallic foam formation", submitted.

44. A. E. Simone, L. J. Gibson, "Aluminum foams produced by liquid-state processes", Acta Mater., 26 (1998) 3109-3123.

45. L. J. Gibson, "Mechanical behavior of metallic foams", Annu. Rev. Mater. Sci., 30 (2000) 191-227.

46. M. C. Shaw, in Mechanical Behavior of Materials, F. A. McClintock and A. S. Argon (eds), Addison-Wesley, Reading, Mass, 1966, p. 443.

47. V. C. Nardone and K. M. Prewo, Scripta Metall., " On the strength of discontinuous silicon carbide reinforced aluminum composites", 20 (1986) 43.

48. W. S. Miller and F. J. Humphreys, Scripta Metall., " Strengthening mechanisms in particulate metal matrix composites"25 (1991) 33.

49. T. W. Clyne, P. J. Withers, "An introduction to metal matrix composites", Cambridge University Press, Cambridge, 1993.

50. J. Sarkar, Scripta Metall., 32 (1995) 37.

51. M. Güden, "High strain rate mechanical behavior of metal matrix composite", Ph. D. Thesis, University of Delaware, 1998.

APPENDIX A

GIBSON AND ASHBY'S SIMPLE CUBIC MODELS FOR OPEN AND CLOSED-CELL FOAMS

Elastic Deformation

Compressive force causes the non-vertical beams to deflect by an amount of δ, (Figure A.1 (a) and (b)) which can be calculated from elastic beam theory as,

$$\delta = \frac{C_1 F l^3}{E_s I} \tag{A.1}$$

where C_1, F, l, E_s and I are cell geometrical factors, applied force, cell wall length or size, cell wall material elastic modulus and second moment area of cell wall or edge, respectively. Force and deflection may be expressed in terms of stress (σ) and strain (ε) as

$$F \propto \sigma l^2 \tag{A.2}$$

and

$$\varepsilon \propto \frac{\delta}{l} \tag{A.3}$$

respectively. The second moment area of cell edge with section t is proportional to t^4 for an open cell and to lt^3 for a closed-cell foam. Placing all variables into Equation A.1 will give the Elastic Modulus, E^* ,as

$$E^* \propto E_s \left(\frac{t}{l}\right)^4 \tag{A.4}$$

for an open cell and

$$E^* \propto E_s \left(\frac{t}{l}\right)^3 \tag{A.5}$$

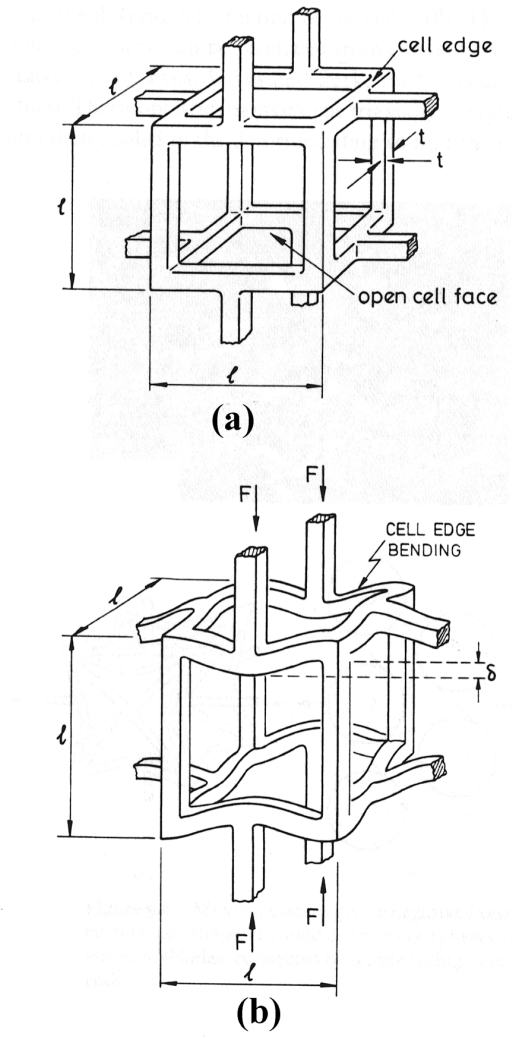

Figure A.1 a) simple cubic model for an open cell and b) model for compression.

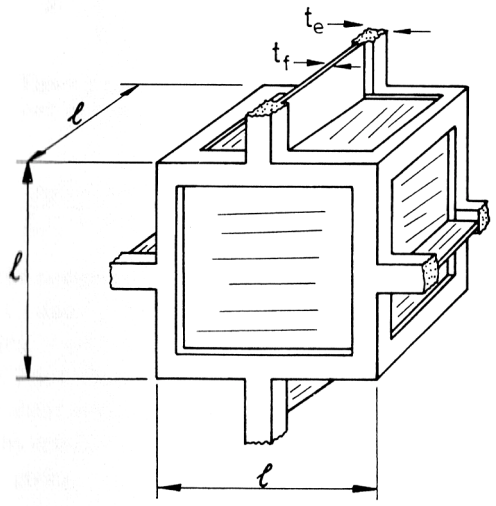

Figure A.2 Cubic model for a closed-cell foam

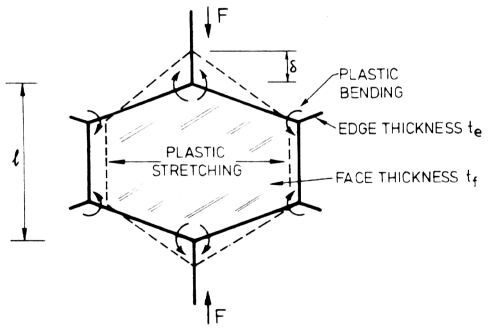

Figure A.3 Model showing plastic stretching of cell faces of a closed-cell.

for a closed-cell foam. The relative densities of open and closed-cell foams are

$$\frac{\rho^*}{\rho_s} \propto \left(\frac{t}{l}\right)^2 \tag{A.6}$$

and

$$\frac{\rho^*}{\rho_s} \propto \left(\frac{t}{l}\right) \tag{A.7}$$

respectively. Therefore Equations A.4 and A.5 are rearranged as

$$\frac{E^*}{E_s} = C_2 \left(\frac{\rho^*}{\rho_s}\right)^2 \tag{A.8}$$

for open cell and

$$\frac{E^*}{E_s} = C_3 \left(\frac{\rho^*}{\rho_s}\right) \tag{A.9}$$

for close-cell foams. In these equations, C_2 and C_3 are geometrical constants.

Besides cell wall bending, there are two other mechanisms which can contribute to the modulus of a closed-cell foam. These are cell face or membrane stretching and enclosed gas pressure. When the foam is formed from a liquid, surface tension can draw much of the liquid to the cell edges (Figure A.2). As a result, a thinner layer material accumulates on the cell faces. This thin layer may rupture easily during bending of cell edges. If not, it will have a significant contribution to the stiffness of the foam as it stretches in a direction 90^o to the compression load axis. Figure A.3 shows

the stretching of a closed-cell upon the application compressive force F. For this figure total elastic strain energy will be a combination of cell edge bending and cell face stretching energies, which is given as,

$$\frac{1}{2}F\delta = \frac{1}{2}S\delta^2 + \frac{1}{2}E_s\varepsilon^2 V_f \qquad (A.10)$$

where S is stiffness of the cell edge ($\alpha E_s l/l^3$), ε is the strain caused by stretching of a cell face and V_f is the volume of solid in a cell face and t_e and t_r are thicknesses of the cell edge and cell face, respectively. Equation A.10 may be also written as

$$\frac{1}{2}F\delta = \frac{\alpha E_s I\delta^2}{l^3} + \beta E_s \left(\frac{\delta}{l}\right)^2 l^2 t_f \qquad (A.11)$$

Using $I\alpha t_e^4$ and $E^* \alpha (F/l^2)(\delta/l)$, equation A.11 can be expressed as

$$\frac{E^*}{E_s} = \alpha' \frac{t_e^4}{l^4} + \beta' \frac{t_f}{l} \qquad (A.12)$$

If the fraction of solid contained in the cell edges (φ) is taken as t_e/l, then Equation A.12 will be

$$\frac{E^*}{E_s} = C_1\varphi^2\left(\frac{\rho}{\rho_s}\right)^2 + C_1(1-\varphi)\left(\frac{\rho}{\rho_s}\right) \qquad (A..13)$$

Equation A.13 describes the combining effects of cell edge bending and cell face stretching together. When the compressed gas is important, the following equation is proposed [1];

$$\frac{E^*}{E_s} = C_1\varphi^2\left(\frac{\rho}{\rho_s}\right)^2 + C_1(1-\varphi)\left(\frac{\rho}{\rho_s}\right) + \frac{P_o(1-2v^*)}{E_s(1-\frac{\rho}{\rho_s})} \qquad (A.14)$$

where P_o and v^* are initial gas pressure and Poisson's ratio of the foam, respectively.

Plastic Collapse

For a closed-cell foam, plastic collapse causes the membranes to crumple in the compression direction with a very small force but the membranes stretch at right angles to this direction. The later process requiring plastic work may significantly contribute to yield strength of the foam. Therefore the total work done can be written as

$$F\delta = \alpha M_p \frac{\delta}{l} + \beta \sigma_y \delta t_f l \qquad \text{(A.15)}$$

where M_p and σ_{ys} are the plastic moment of the cell edges and the yield strength of the foam material respectively. Replacing F by σl^2 and M_p by $\sigma_{ys} t_e^3/4$ gives

$$\frac{\sigma_{pl}^*}{\sigma_{ys}} = C_5 \left(\varphi \frac{\rho^*}{\rho_s} \right)^{3/2} + C_5'' (1-\varphi) \left(\frac{\rho^*}{\rho_s} \right) \qquad \text{(A.16)}$$

Equation A.16 can be further arranged by including compressed gas contribution as

$$\frac{\sigma_{pl}^*}{\sigma_{ys}} = C_5 \left(\varphi \frac{\rho^*}{\rho_s} \right)^{3/2} + C_5'' (1-\varphi) \left(\frac{\rho^*}{\rho_s} \right) + \frac{P_o - P_{atm}}{\sigma_{ys}} \qquad \text{(A.17)}$$

For an open cell, φ=1, Equation A.16 gives

$$\frac{\sigma_{pl}^*}{\sigma_{ys}} = C_5 \left(\frac{\rho^*}{\rho_s} \right)^{3/2} \qquad \text{(A.18)}$$

And for an closed-cell, φ=0, Equation A.16 gives,

$$\frac{\sigma_{pl}^{*}}{\sigma_{ys}} = C_5'' \left(\frac{\rho^{*}}{\rho_s} \right) \tag{A.19}$$

Therefore, Equation A.18 and A.19 can be used to predict the plateau stresses of open and closed-cell foams, respectively.

APPENDIX B

EXPERIMENTAL FOAMING RESULTS

Table B.1 Foaming experiment data for Al compacts

Specimen Code	Initial Height (mm)	Temperature (^{o}C)	Final Height (mm)	Time (minute)
UF 1	9.92	750	44.81	10.00
UF 2	9.83	750	14.40	6.00
UF 3	9.81	750	36.57	8.00
UF 4	9.80	750	28.10	9.00
UF 5	9.80	750	41.19	9.00
UF 6	9.89	750	29.85	7.00
UF 7	9.83	750	42.21	20.00
UF 8	9.80	850	41.87	8.00
UF 9	9.82	850	42.28	6.00
UF 10	9.81	850	42.05	5.00
UF 11	9.88	850	37.71	4.30
UF 12	9.80	850	0.00	4.00
UF 13	9.82	750	39.83	12.00
UF 14	9.85	750	41.21	15.00
UF 15	9.81	850	30.81	4.00
UF 16	9.82	850	27.95	3.30
UF 17	9.85	850	36.66	5.30
UF 18	9.82	850	28.35	5.00
UF 19	9.80	850	36.05	5.00
UF 20	9.78	750	35.15	8.30
UF 21	9.70	750	44.98	7.00
UF 22	9.70	750	44.45	10.00
UF 23	9.75	750	43.70	20.00
UF 24	9.70	750	47.65	6.00
UF 25	9.65	750	21.50	5.00
UF 26	9.63	750	29.89	5.30
UF 27	9.63	750	46.22	6.30
UF 28	9.67	750	46.19	6.00
UF 29	9.68	750	45.85	7.00

UF refers to "*Unreinforced Al Foam*"

Table B.2 Foaming experiment data for 8.6% Al_2O_3 and 8.6% and 20% SiC_p/Al compacts.

Specimen Code	Initial Height (mm)	Temperature (^oC)	Final Height (mm)	Time (minute)
Al-Al_2O_3-8.6%-1	9.64	750	45.64	8.30
Al-Al_2O_3-8.6%-2	9.75	750	49.51	7.00
Al-Al_2O_3-8.6%-3	9.55	750	42.40	6.30
Al-SiC_P-8.6%-1	9.33	850	46.90	4.30
Al-SiC_P-8.6%-2	9.51	750	63.40	8.00
Al-SiC_P-8.6%-3	9.46	750	54.52	8.00
Al-SiC_P-8.6%-4	9.33	750	60.42	7.00
Al-SiC_P-8.6%-5	9.25	750	55.56	6.00
Al-SiC_P-8.6%-6	9.40	750	16.76	5.00
Al-SiC_P-8.6%-7	9.28	750	26.50	5.30
Al-SiC_P-8.6%-8	9.36	750	29.80	5.45
Al-SiC_P-8.6%-9	9.28	750	49.25	15.00
Al-SiC_P-8.6%-10	9.41	750	56.66	7.00
Al-SiC_P-8.6%-11	9.26	750	36.86	6.45
Al-SiC_P-8.6%-12	9.45	750	57.30	5.30
Al-SiC_P-8.6%-13	9.45	750	57.91	5.45
Al-SiC_P-20%-1	9.35	750	51.80	6.00
Al-SiC_P-20%-2	9.40	750	59.03	6.30